

STARS Enabled Integrated Sensing and Communications

Zhaolin Wang, *Graduate Student Member, IEEE*, Xidong Mu, *Member, IEEE*,
and Yuanwei Liu, *Senior Member, IEEE*

Abstract

A simultaneously transmitting and reflecting intelligent surface (STARS) enabled integrated sensing and communications (ISAC) framework is proposed, where the whole space is divided by STARS into a sensing space and a communication space. A novel sensing-at-STARS structure, where dedicated sensors are installed at the STARS, is proposed to address the significant path loss and clutter interference for sensing. The Cramér-Rao bound (CRB) of the 2-dimension (2D) direction-of-arrivals (DOAs) estimation of the sensing target is derived, which is then minimized subject to the minimum communication requirement. A novel approach is proposed to transform the complicated CRB minimization problem into a trackable modified Fisher information matrix (FIM) optimization problem. Both independent and coupled phase-shift models of STARS are investigated: 1) For the independent phase-shift model, to address the coupling of ISAC waveform and STARS coefficient in the modified FIM, an efficient double-loop iterative algorithm based on the penalty dual decomposition (PDD) framework is conceived; 2) For the coupled phase-shift model, based on the PDD framework, a low complexity alternating optimization algorithm is proposed to tackle coupled phase-shift constants by alternatively optimizing amplitude and phase-shift coefficients in closed-form. Finally, the numerical results demonstrate that: 1) STARS significantly outperforms the conventional RIS in CRB under the communication constraints; 2) The coupled phase-shift model achieves comparable performance to the independent one for low communication requirements or sufficient STARS elements; 3) It is more efficient to increase the number of passive elements of STARS rather than the active elements of the sensor; 4) High sensing accuracy can be achieved by STARS using the practical 2D maximum likelihood estimator compared with the conventional RIS.

Index Terms

Cramér-Rao bound, integrated sensing and communication (ISAC), simultaneously transmitting and reflecting intelligent surface (STARS).

Zhaolin Wang, Xidong Mu, and Yuanwei Liu are with the School of Electronic Engineering and Computer Science, Queen Mary University of London, London E1 4NS, U.K. (e-mail: zhaolin.wang@qmul.ac.uk, xidong.mu@qmul.ac.uk, yuanwei.liu@qmul.ac.uk).

I. INTRODUCTION

Integrated sensing and communications (ISAC) technique has been recognized as an important enabler of the next-generation wireless networks [1]. The goal of ISAC is to integrate sensing function and communication function within a single platform to share the same resources, hardware facilities, and signal processing modules. Apart from the apparent benefits such as high spectral, energy, and hardware efficiency, ISAC also empowers wireless networks to be aware of the surrounding environment for establishing ubiquitous intelligence in the future smart world [2]. This opens exciting opportunities for developing environment-aware techniques, including but not limited to augmented reality (AR), virtual reality (VR), and vehicle to everything (V2X). Moreover, by copying the physical world via sensing and exchanging information via communication, ISAC can bridge the virtual and physical worlds and build the foundation of Metaverse [3].

Reconfigurable intelligent surface (RIS) is another promising technique for achieving a smart radio environment of the next-generation wireless networks [4]. On the one hand, RIS is capable of dynamically adjusting its passive beamforming to enhance communication performance. On the other hand, RIS can also establish a line-of-sight (LoS) link with the target to facilitate sensing performance. However, the conventional transmitting/reflecting-only RIS requires the sensing targets or the communication users to be located at the same side of the RIS as the base station (BS), which can only achieve half-space coverage. To address this challenge, a promising simultaneous transmitting and reflecting intelligent surface (STARS) is recently proposed to realize 360° full-space coverage [5]. As a consequence, STARS is capable of providing new degrees of freedom (DoFs), namely both transmission and reflection beamforming [6], for enhancing both sensing and communication performance.

A. Prior Works

There have been growing research interests in the ISAC from various perspectives in recent years. With the rapid development of multiple-input multiple-out (MIMO) techniques, the higher DoFs can be provided by the multi-antenna arrays for constructing highly directional beams toward the communication users and the sensing targets, which motivates many works to investigate ISAC from the transmit beamforming perspective [7]–[10]. Specifically, following a path from partially to fully shared antenna arrays, the authors of [7] jointly designed the transmit beamforming to approach the desired sensing beampattern while guaranteeing the minimum communication signal-to-interference-plus-noise-ratio (SINR) requirements. As a further

advance, authors of [8] proposed to add the additional dedicated sensing signals for compensating the DoFs degradation caused by the limited number of communication users, which also lights a path to the optimal transmit beamforming design. To enhance the design flexibility between communication and sensing subsystems, several transmit beamforming designs were proposed in [9] for guaranteeing the user-prescribed levels of sensing and communication performance. Furthermore, an ISAC system based on metamaterial antennas, which is capable of supporting ultra-dense radiation elements, was conceived in [10], where a holographic transmit beamforming scheme was proposed.

Although the aforementioned transmit beamforming designs is capable of realizing a favorable trade-off between sensing and communication, the sensing performance is not fully considered. Note that the sensing function is executed by transmitting signals to the target and then analyzing the received echo signals reflected by the target, indicating that the sensing performance is mainly characterized at the receiver side and that designing the transmit beamforming alone is not sufficient. As a remedy, by considering the echo signals, some works employed the general sensing SINR [11] or the general sensing mutual information (MI) [12] as the performance metric, leading to the joint transceiver design. In the meantime, from the perspective of estimation accuracy of sensing function, the fundamental Cramér-Rao bound (CRB), which characterizes the minimum achievable variance of the unbiased estimators at the receiver, was considered in the recent works of ISAC [13], [14]. In particular, the two optimization frameworks for minimizing the CRB for estimating the parameters of point target and extended target were proposed in [13], where the optimal transmit beamforming was obtained via semidefinite relaxation (SDR). Furthermore, the authors of [14] investigated the optimal trade-off region of the CRB and communication rate of an ISAC system with one extended target and one multi-antenna user.

Recently, motivated by the capability of RIS to adjust the signal propagation environment and significantly improve the performance of wireless communication [15]–[17], the RIS-assisted wireless sensing techniques have received growing attention [18]–[20]. In [18], the authors employed RIS to facilitate the multi-target detection by jointly optimizing the sensing waveform and the RIS phase-shifts. However, due to the long round-trip distance and multiple hops through the path between BS, RIS, and target, the sensing performance is limited by the significant path loss in the RIS-assisted sensing system. Hence, the authors of [19] proposed a RIS-self-sensing scheme, where the probing signal is emitted from a co-located RIS controller and the echo signal is analyzed at the low-cost active sensors installed on the RIS. Furthermore, the

authors of [20] studied the RIS-assisted sensing from the CRB perspective, where the CRB for estimating the azimuth direction-of-arrival (DOA) of one target is derived and is then minimized by jointly designing the active and passive beamforming. There also have been extensive research contributions to RIS-assisted ISAC techniques. For example, two joint active and passive beamforming designs were proposed in [21] for ISAC systems assisted by the single RIS and the dual RISs, respectively. The authors of [22] jointly optimized the transmit waveform and passive beamforming to maximize the sensing SINR achieved by the space-time adaptive processing at the BS subject to different communication constraints. To guarantee the estimation accuracy, the authors of [23] proposed to minimize the multi-user interference of communication under the minimum CRB requirement of sensing.

B. Motivations and Challenges

The motivations of this paper can be summarized in three folds as follows.

- 1) In contrast to conventional RIS, STARS does not require the sensing target and the communicating user to be on the same side. Moreover, STARS can split one signal into two separate signals, which matches well with the dual functions in ISAC. Driven by the above observations, in this paper, we naturally propose to employ STARS to divide the whole space into two half-spaces, namely the *sensing space* and the *communication space*. Therefore, the signal from the BS is split at the STARS to carry out target sensing at the sensing space and serve communication users at the communication space, namely ISAC is *enabled* by the STARS.
- 2) Typically, the sensing function is carried out at the BS by analyzing the echo signals from the target. However, the following challenges need to be solved when STARS is exploited. On the one hand, the sensing signal experiences significant path loss over multiple hops, i.e., $\text{BS} \rightarrow \text{STARS} \rightarrow \text{target} \rightarrow \text{STARS} \rightarrow \text{BS}$, especially when the direct BS-target link is blocked and the STARS is deployed in the vicinity of the target. On the other hand, due to the transmission and reflection property of STARS, the BS can also receive clutter signals from the communication space, which is difficult to be identified with desired echo signals from the sensing space. To tackle these challenges, we propose to install the dedicated low-cost sensors on the STARS following a similar idea of [19]. Thus, the sensing function can be carried out at these sensors, namely *sensing-at-STARS*, rather than at the BS, leading to fewer hops and lower path loss. Furthermore, to avoid the clutter signal from the communication space, the side of the sensor facing the communication

space can be physically blocked. In this case, the sensors can only receive the echo signals from the sensing space.

- 3) Finally, since the effectiveness of optimizing the CRB has been widely proved, we also considered it as the performance metric of sensing. However, in the existing works [13], [19], [20], [23], only the estimation of the azimuth DOA of the target is studied. Note that the RIS or STARS are usually equipped with the uniform planar array (UPA), which is capable of estimating both azimuth and elevation DOAs. This motivates us to investigate the CRB of the 2-dimension (2D) DOA estimation in this paper.

C. Contributions

The primary contributions of our paper are summarized as follows:

- We propose a novel STARS-enabled ISAC system with a sensing-at-STARS structure, where the whole space is divided into a sensing space with a single target and a communication space with multiple users. Based on this setup, we derive the CRB for estimating the 2D DOAs of the target. Considering both independent and coupled phase-shift models of STARS, we formulate the CRB minimization problem under the communication SINR constraints.
- For the independent phase-shift model, instead of directly minimizing the complicated CRB, we propose to equivalently optimize a modified Fisher information matrix (FIM). Furthermore, we propose a penalty dual decomposition (PDD)-based algorithm to address the coupling modified FIM.
- For the coupled phase-shift model, to tackle the additional complicated non-convex coupled phase-shift constraints, we conceive a low complexity algorithm by optimizing the amplitude and phase-shift coefficients of STARS iteratively, where the optimal closed-form solution of each iteration is derived.
- Our numerical results verify the effectiveness of the proposed algorithms and unveil the superior of the STARS over the conventional RIS in terms of ISAC performance both theoretically and practically. Some insights are also obtained from the numerical results. Firstly, the two coupled phase-shift models have similar performance in the case of low communication requirements or sufficient STARS elements. Secondly, compared with the number of sensor elements, increasing the number of passive elements of STARS is more appealing.

D. Organization and Notations

The rest of this paper is organized as follows. In Section II, the proposed STARS-enabled ISAC framework with the sensing-at-STARS structure is presented. Then, the CRB for the 2D DOA estimation is derived. In Section III, a PDD-based algorithm is conceived to solve the CRB minimization problem with the independent phase-shift model, where a novel CRB simplification approach is proposed. In Section IV, considering the coupled phase-shift model, another PDD-based algorithm is proposed to solve the corresponding CRB minimization problem, where the coupled phase-shift constraints are addressed in an alternating manner based on the optimal closed-form solutions. In Section V, the numerical results are provided to verify the effectiveness of the proposed framework and algorithms. Finally, this paper is concluded in Section VI

Notations: Scalars, vectors, and matrices are denoted by the lower-case, bold-face lower-case, and bold-face upper-case letters, respectively; $\mathbb{C}^{N \times M}$ and $\mathbb{R}^{N \times M}$ denotes the space of $N \times M$ complex and real matrices, respectively; a^* and $|a|$ denote the conjugate and magnitude of scalar a ; \mathbf{a}^H denotes the conjugate transpose of vector \mathbf{a} ; $\text{diag}(\mathbf{a})$ denotes a diagonal matrix with same value as the vector \mathbf{a} on the diagonal; $\mathbf{A} \succeq 0$ means that matrix \mathbf{A} is positive semidefinite; $\text{rank}(\mathbf{A})$ and $\text{tr}(\mathbf{A})$ denote the rank and trace of matrix \mathbf{A} , respectively; $\mathbb{E}[\cdot]$ denotes the statistical expectation; $\text{Re}\{\cdot\}$ denotes the real component of a complex number; $\mathcal{CN}(\mu, \sigma^2)$ denotes the distribution of a circularly symmetric complex Gaussian (CSCG) random variable with mean μ and variance σ^2 ; \odot denotes the Hadamard product.

II. SYSTEM MODEL

As shown in Fig. 1, we consider a STARS-enabled ISAC system, where the BS is equipped with a uniform linear array (ULA) consisting of M antennas and the STARS is equipped with a uniform planar array (UPA) consisting of N transmission-reflection (T-R) elements denoted by the set \mathcal{N} . The whole space is divided into two half-spaces by STARS, namely the *sensing space* and the *communication space*. Without loss of generality, we assume that the sensing space is on the reflection side and the communication space is on the transmission side. There is one sensing target of interest in the sensing space and K single-antenna communication users denoted by the set \mathcal{K} in the communication space. The direct links between BS and target/users are assumed to be blocked. To tackle the severe path-loss, we propose a sensing-at-STARS structure by installing the dedicated low-cost sensors with a ULA consisting of N_s elements at the STARS to carry out target sensing. Furthermore, to avoid the clutter signal from the communication space, we assume that the side of the sensor facing the communication space is physically blocked.

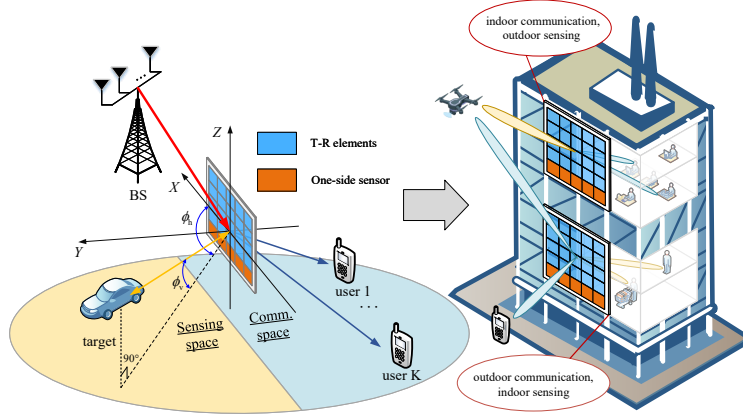


Fig. 1: Illustration of the STARS-enabled ISAC system.

A. STARS Model

The energy splitting model is exploited for supporting simultaneous transmission and reflection of the STARS. In particular, the incident signal at the STARS from the BS is split into the sensing signal in the sensing space and the communication signal in the communication space. Let $\Theta_t \in \mathbb{C}^{N \times N}$ and $\Theta_r \in \mathbb{C}^{N \times N}$ denotes the matrices of the transmission coefficients (TCs) and reflection coefficients (RCs), respectively, which can be modeled as

$$\Theta_i = \text{diag}(\beta_{i,1}e^{j\varphi_{i,1}}, \dots, \beta_{i,N}e^{j\varphi_{i,N}}), \quad \forall i \in \{t, r\}. \quad (1)$$

In the above expression, $\beta_{i,n} \in [0, 1]$ and $\varphi_{i,n} \in [0, 2\pi)$ denote the amplitude and phase-shift response of the n -th element. The exact value of $\beta_{i,n}$ and $\varphi_{i,n}$ is determined by the resistance and reactance of the STARS element. Generally, it is assumed that the phase-shifts of TCs and RCs can be independently adjusted and the amplitudes are coupled by the *law of energy conservation* as follows:

$$\beta_{t,n}^2 + \beta_{r,n}^2 = 1, 0 \leq \beta_{t,n}, \beta_{r,n} \leq 1, \forall n \in \mathcal{N}, \quad (2)$$

which is termed as *independent T&R phase-shift model*. The independent T&R phase-shift model requires the STARS elements to be active or lossy [24], which may lead to a higher manufacturing cost. However, when the STARS are passive and lossless, the following conditions also need to be satisfied for the TCs and RCs [24]:

$$\beta_{t,n}\beta_{r,n}\cos(\varphi_{t,n} - \varphi_{r,n}) = 0, \forall n \in \mathcal{N}. \quad (3)$$

In the above constraints, the phase-shifts of TCs and RCs are also coupled, which is termed as *coupled T&R phase-shift model*. To fully investigate the role that STARS plays in the proposed ISAC system, both the independent and coupled T&R phase-shift models are also considered in this paper.

B. Signal Model

To carry out sensing and communication simultaneously, the BS transmits the following joint signal at the t -th time index:

$$\mathbf{x}(t) = \mathbf{P}\mathbf{c}(t) + \mathbf{s}(t) = \sum_{k=1}^K \mathbf{p}_k c_k(t) + \mathbf{s}(t), \quad (4)$$

where $\mathbf{P} = [\mathbf{p}_1, \dots, \mathbf{p}_K] \in \mathbb{C}^{M \times K}$ denotes the transmit beamformers for delivering the information streams $\mathbf{c}(t) = [c_1(t), \dots, c_K(t)]^T \in \mathbb{C}^{K \times 1}$ to K communication users. The signal $\mathbf{s}(t)$ is the dedicated sensing signal for achieving the full DoFs of target sensing. The multiple beam transmission is exploited by the dedicated sensing signal, namely $\mathbf{s}(t) = \sum_{i=1}^{\mathcal{E}_s} \tilde{\mathbf{s}}_i(t)$. Thus, the covariance matrix of it, namely $\mathbf{R}_S = \mathbb{E}[\mathbf{s}(t)\mathbf{s}(t)^H]$, is with general rank. Furthermore, the communication signals are modeled as independent Gaussian random signals with zero mean and unit power, namely $\mathbb{E}[\mathbf{c}(t)\mathbf{c}(t)^H] = \mathbf{I}_K$ and $\mathbb{E}[\mathbf{c}(t)\mathbf{s}(t)^H] = \mathbf{0}_{K \times M}$. Based on this, the covariance matrix of the transmit signal $\mathbf{x}(t)$ is given by

$$\mathbf{R}_X = \mathbb{E}[\mathbf{x}(t)\mathbf{x}(t)^H] = \mathbf{P}\mathbf{P}^H + \mathbf{R}_S. \quad (5)$$

In practice, \mathbf{R}_X can be calculated over L time indexes, namely

$$\mathbf{R}_X \approx \frac{1}{L} \mathbf{X}\mathbf{X}^H, \quad (6)$$

where $\mathbf{X} = [\mathbf{x}(1), \dots, \mathbf{x}(L)]$. The above approximation is accurate when L is large. Thus, we assume the accurate equality of (6) is achieved throughout this paper.

Given the transmit signal at the BS, the received signal at the k -th communication user in the communication space can be modeled as

$$y_{c,k}(t) = \underbrace{\mathbf{h}_k^H \mathbf{\Theta}_t \mathbf{H} \mathbf{p}_k c_k(t)}_{\text{desired signal}} + \underbrace{\sum_{i=1, i \neq k}^K \mathbf{h}_k^H \mathbf{\Theta}_t \mathbf{H} \mathbf{p}_i c_i(t)}_{\text{inter-user interference}} + \underbrace{\mathbf{h}_k^H \mathbf{\Theta}_t \mathbf{H} \mathbf{s}(t)}_{\text{sensing interference}} + n_k(t), \quad (7)$$

where $\mathbf{H} \in \mathbb{C}^{N \times M}$ denotes the BS to STRA-RIS channel, $\mathbf{h}_k \in \mathbb{C}^{N \times 1}$ denotes the STARS to user k channel, and $n_k \sim \mathcal{CN}(0, \sigma_k^2)$ denotes the additive white Gaussian noise (AWGN) with covariance σ_k^2 . Then, in the sensing space, the reflected echo signal over the sensing dwell time L from the target to the sensor can be modeled as

$$\mathbf{Y}_s = \alpha \mathbf{b}(\phi_h, \phi_v) \mathbf{a}^T(\phi_h, \phi_v) \mathbf{\Theta}_r \mathbf{H} \mathbf{X} + \mathbf{N}_s, \quad (8)$$

where $\alpha \in \mathbb{C}$ includes both round-trip path-loss and the complex reflection factor of the target, ϕ_h and ϕ_v denotes azimuth and elevation angles of the target related to the STARS and sensor, $\mathbf{a}(\phi_h, \phi_v)$ denotes the steering vector of the STARS, $\mathbf{b}(\phi_h, \phi_v)$ denotes the steering vector of the sensor, and \mathbf{N}_s denotes the AWGN noise with the variance of each entries being σ_s^2 . According

to [25], the steering vectors can be modeled as

$$\mathbf{a}(\phi_h, \phi_v) = \exp(-j[\mathbf{r}_X, \mathbf{r}_Y, \mathbf{r}_Z]\mathbf{k}(\phi_h, \phi_v)), \quad (9)$$

$$\mathbf{b}(\phi_h, \phi_v) = \exp(-j[\bar{\mathbf{r}}_X, \bar{\mathbf{r}}_Y, \bar{\mathbf{r}}_Z]\mathbf{k}(\phi_h, \phi_v)), \quad (10)$$

where $[\mathbf{r}_X, \mathbf{r}_Y, \mathbf{r}_Z] \in \mathbb{R}^{N \times 3}$ and $[\bar{\mathbf{r}}_X, \bar{\mathbf{r}}_Y, \bar{\mathbf{r}}_Z]^{N_s \times 3}$ have rows representing the Cartesian coordinates of the STARS and sensor elements, and $\mathbf{k}(\phi_h, \phi_v)$ denotes the wavenumber vector:

$$\mathbf{k}(\phi_h, \phi_v) = \frac{2\pi}{\lambda_c} [\cos \phi_h \cos \phi_v, \sin \phi_h \cos \phi_v, \sin \phi_v]^T, \quad (11)$$

where λ_c denotes the wavelength of the carrier signal. Without loss of generality, we assume that the ULA array of the sensor is deployed along the X -axis and the UPA array of the STARS is deployed within the (X, Z) plane, namely $\bar{\mathbf{r}}_Y = \bar{\mathbf{r}}_Z = \mathbf{0}$ and $\mathbf{r}_Y = \mathbf{0}$. As a consequence, the steering vectors can be simplified as follows:

$$\mathbf{a}(\phi_h, \phi_v) = \exp\left(-j\frac{2\pi}{\lambda_c}(\mathbf{r}_X \cos \phi_h \cos \phi_v + \mathbf{r}_Z \sin \phi_v)\right), \quad (12)$$

$$\mathbf{b}(\phi_h, \phi_v) = \exp\left(-j\frac{2\pi}{\lambda_c}\bar{\mathbf{r}}_X \cos \phi_h \cos \phi_v\right), \quad (13)$$

C. Performance Metrics for Communication and 2D Sensing

For communication, we exploit the classical SINR as the performance metric. According to (7), the SINR for decoding the desired signal of user k is given by

$$\gamma_k = \frac{|\mathbf{h}_k^H \boldsymbol{\Theta}_t \mathbf{H} \mathbf{p}_k|^2}{\sum_{i \in \mathcal{K}, i \neq k} |\mathbf{h}_k^H \boldsymbol{\Theta}_t \mathbf{H} \mathbf{p}_i|^2 + \mathbf{h}_k^H \boldsymbol{\Theta}_t \mathbf{H} \mathbf{R}_S \mathbf{H}^H \boldsymbol{\Theta}_t^H \mathbf{h}_k + \sigma_k^2}. \quad (14)$$

For the sensing, we are interested in characterizing the CRB for estimating the 2D DOAs ϕ_h and ϕ_v . By vectorizing the matrix \mathbf{Y}_s , we have

$$\mathbf{y}_s = \text{vec}(\mathbf{Y}_s) = \mathbf{u} + \mathbf{n}_s, \quad (15)$$

where $\mathbf{u} = \text{vec}(\alpha \mathbf{b}(\phi_h, \phi_v) \mathbf{a}^T(\phi_h, \phi_v) \boldsymbol{\Theta}_r \mathbf{H} \mathbf{X})$ and $\mathbf{n}_s = \text{vec}(\mathbf{N}_s)$. Let $\boldsymbol{\xi} = [\phi^T, \tilde{\alpha}^T]^T$, where $\phi = [\phi_h, \phi_v]^T$ and $\tilde{\alpha} = [\text{Re}(\alpha), \text{Im}(\alpha)]^T$, denotes the unknown parameters to estimate and \mathbf{J}_ξ denotes FIM for estimating $\boldsymbol{\xi}$ from \mathbf{y}_s . Note that \mathbf{y}_s is essentially a Gaussian observation with the distribution $\mathbf{y}_s \sim \mathcal{CN}(\mathbf{u}, \mathbf{R}_{\mathbf{n}_s})$, where $\mathbf{R}_{\mathbf{n}_s} = \sigma_s^2 \mathbf{I}_{N_S L}$ denotes the covariance matrix of \mathbf{n}_s . Then, following the same path in [26, Appendix 3C], the (l, p) -th element of \mathbf{J}_ξ can be calculated by

$$[\mathbf{J}_\xi]_{l,p} = 2\text{Re} \left\{ \frac{\partial \mathbf{u}^H}{\partial \xi_l} \mathbf{R}_{\mathbf{n}_s}^{-1} \frac{\partial \mathbf{u}}{\partial \xi_p} \right\} + \text{tr} \left(\mathbf{R}_{\mathbf{n}_s}^{-1} \frac{\partial \mathbf{R}_{\mathbf{n}_s}}{\partial \xi_l} \mathbf{R}_{\mathbf{n}_s}^{-1} \frac{\partial \mathbf{R}_{\mathbf{n}_s}}{\partial \xi_p} \right) = \frac{2}{\sigma_s^2} \text{Re} \left\{ \frac{\partial \mathbf{u}^H}{\partial \xi_l} \frac{\partial \mathbf{u}}{\partial \xi_p} \right\} \quad (16)$$

As a consequence, \mathbf{J}_ξ can be partitioned as

$$\mathbf{J}_\xi = \begin{bmatrix} \mathbf{J}_{\phi\phi} & \mathbf{J}_{\phi\tilde{\alpha}} \\ \mathbf{J}_{\phi\tilde{\alpha}}^T & \mathbf{J}_{\tilde{\alpha}\tilde{\alpha}} \end{bmatrix}. \quad (17)$$

Then, the CRB matrix for estimating the DOAs ϕ can be expressed as [27]

$$\text{CRB}(\phi) = [\mathbf{J}_{\phi\phi} - \mathbf{J}_{\phi\tilde{\alpha}}\mathbf{J}_{\tilde{\alpha}\tilde{\alpha}}^{-1}\mathbf{J}_{\phi\tilde{\alpha}}^T]^{-1}, \quad (18)$$

where the expressions of the matrices $\mathbf{J}_{\phi\phi}$, $\mathbf{J}_{\phi\tilde{\alpha}}$, and $\mathbf{J}_{\tilde{\alpha}\tilde{\alpha}}$ are derived in Appendix A.

III. CRB OPTIMIZATION DESIGN WITH INDEPENDENT T&R PHASE-SHIFT

In this section, based on the proposed framework, we focus on the optimization of CRB with independent T&R phase-shift, which can be simplified to the optimization of a modified FIM. Then, we propose to solve the resultant optimization problem by invoking the PDD framework.

A. Problem Formulation

It is well known that the diagonal elements of the CRB matrix represent the minimum variance for estimating each parameter via unbiased estimators. Therefore, we aim to minimize the trace of the CRB matrix, while guaranteeing the minimum communication SINR. However, the CRB matrix $\text{CRB}(\phi)$ is too complicated. In this case, we use the following proposition to transform it into a more trackable form.

Proposition 1. Minimizing the trace of CRB matrix $\text{CRB}(\phi)$ is equivalent to solving the following optimization problem

$$\min \quad \text{tr}(\mathbf{U}^{-1}) \quad (19a)$$

$$\text{s.t.} \quad \begin{bmatrix} \mathbf{J}_{\phi\phi} - \mathbf{U} & \mathbf{J}_{\phi\tilde{\alpha}} \\ \mathbf{J}_{\phi\tilde{\alpha}}^T & \mathbf{J}_{\tilde{\alpha}\tilde{\alpha}} \end{bmatrix} \succeq 0, \quad (19b)$$

$$\mathbf{U} \succeq 0. \quad (19c)$$

Proof. Firstly, we have that the FIM $\mathbf{J}_{\phi\phi} - \mathbf{J}_{\phi\tilde{\alpha}}\mathbf{J}_{\tilde{\alpha}\tilde{\alpha}}^{-1}\mathbf{J}_{\phi\tilde{\alpha}}^T$ is a positive semidefinite matrix. According to [28, Example 3.46], the function $\text{tr}(\mathbf{A}^{-1})$ is matrix decreasing on the positive semidefinite matrix space. Therefore, minimizing $\text{tr}([\mathbf{J}_{\phi\phi} - \mathbf{J}_{\phi\tilde{\alpha}}\mathbf{J}_{\tilde{\alpha}\tilde{\alpha}}^{-1}\mathbf{J}_{\phi\tilde{\alpha}}^T]^{-1})$ is equivalent to minimizing $\text{tr}(\mathbf{U}^{-1})$, where $\mathbf{U} \succeq 0$, subject to the constraint

$$\mathbf{J}_{\phi\phi} - \mathbf{J}_{\phi\tilde{\alpha}}\mathbf{J}_{\tilde{\alpha}\tilde{\alpha}}^{-1}\mathbf{J}_{\phi\tilde{\alpha}}^T \succeq \mathbf{U}. \quad (20)$$

Then, based on the Schur complement condition [29], the constraint (19b) with a modified FIM can be obtained. ■

Based on Proposition 1, the optimization problem for minimizing $\text{CRB}(\phi)$ can be formulated as follows:

$$\mathcal{P} : \quad \min_{\mathbf{U}, \mathbf{P}, \mathbf{R}_S, \theta_t, \theta_r} \quad \text{tr}(\mathbf{U}^{-1}), \quad (21a)$$

$$\text{s.t.} \quad \begin{bmatrix} \mathbf{J}_{\phi\phi} - \mathbf{U} & \mathbf{J}_{\phi\tilde{\alpha}} \\ \mathbf{J}_{\phi\tilde{\alpha}}^T & \mathbf{J}_{\tilde{\alpha}\tilde{\alpha}} \end{bmatrix} \succeq 0, \quad (21b)$$

$$\gamma_k \geq \Gamma, \forall k \in \mathcal{K} \quad (21c)$$

$$\text{tr}(\mathbf{P}\mathbf{P}^H + \mathbf{R}_S) \leq P, \quad (21d)$$

$$\beta_{t,n}^2 + \beta_{r,n}^2 = 1, 0 \leq \beta_{t,n}, \beta_{r,n} \leq 1, \forall n \in \mathcal{N}, \quad (21e)$$

$$\mathbf{R}_S \succeq 0, \mathbf{U} \succeq 0, \quad (21f)$$

where $\boldsymbol{\theta}_i = [\beta_{i,1}e^{j\varphi_{i,1}}, \dots, \beta_{i,N}e^{j\varphi_{i,N}}]^T$, $\forall i \in \{t, r\}$ denotes the entries on the diagonal of matrix $\boldsymbol{\Theta}_i$, $\forall i \in \{t, r\}$, Γ in constraint (21c) denotes the minimum SINR requirement of communication users, and P in constraint (21d) denotes the total power budget at the BS. Constraint (21e) characterizes the amplitude relationships between TCs and RCs. Finally, constraint (21f) ensure the covariance matrix \mathbf{R}_S to be positive semidefinite. The main challenges for solving problem \mathcal{P} is the highly coupled the active beamforming matrices \mathbf{P} , \mathbf{R}_S and the passive beamforming vectors $\boldsymbol{\theta}_t, \boldsymbol{\theta}_r$ in the non-convex constraint (21b) and (21c). As a consequence, it is challenging to find the global optimum to problem \mathcal{P} . However, in the following subsections, we develop an efficient PDD-based algorithm to obtain a high-quality solution to \mathcal{P} .

B. PDD Framework for Solving Problem \mathcal{P}

As shown in [30], standard PDD optimization framework is developed in a double loops structure, where the augmented Lagrangian (AL) problem of the original problem is optimized in a block coordinate descent (BCD) manner in the inner loop while the Lagrangian dual variables and penalty parameters are updated in the outer loop. Therefore, the key idea of applying the PDD method for solving \mathcal{P} is to construct an AL problem of it that has simple or even closed-form solutions at each step of BCD. To this end, we first define the following auxiliary variable:

$$\mathbf{F} = \boldsymbol{\Theta}_r \mathbf{H} \mathbf{R}_X \mathbf{H}^H \boldsymbol{\Theta}_r^H, \quad (22)$$

Then, \mathcal{P} can be reformulated as

$$\min_{\boldsymbol{\chi}} \quad \text{tr}(\mathbf{U}^{-1}) \quad (23a)$$

$$\text{s.t.} \quad \mathbf{F} = \boldsymbol{\Theta}_r \mathbf{H} \mathbf{R}_X \mathbf{H}^H \boldsymbol{\Theta}_r^H, \quad (23b)$$

$$\begin{bmatrix} \mathbf{J}_{\phi\phi}(\mathbf{F}) - \mathbf{U} & \mathbf{J}_{\phi\tilde{\alpha}}(\mathbf{F}) \\ \mathbf{J}_{\phi\tilde{\alpha}}^T(\mathbf{F}) & \mathbf{J}_{\tilde{\alpha}\tilde{\alpha}}(\mathbf{F}) \end{bmatrix} \succeq 0, \quad (23c)$$

$$(21c) - (21f), \quad (23d)$$

Algorithm 1 PDD-based algorithm for solving problem \mathcal{P} .

- 1: Initialize feasible $\mathcal{X}^{[0]}$, $\Upsilon^{[0]}$, $\rho^{[0]} \geq 0$, and set $0 < c < 1$, $n = 1$.
 - 2: **repeat**
 - 3: $\mathcal{X}^{[n+1]} = \text{optimize}(\mathcal{P}_{\text{AL}}(\rho^{[n]}, \Upsilon^{[n]}))$
 - 4: **if** $h(\mathcal{X}^{[n+1]}) \leq \eta^{[n]}$ **then**
 - 5: $\Upsilon^{[n+1]} = \Upsilon^{[n]} + \frac{1}{\rho}(\mathbf{F}^{[n+1]} - \Theta_r^{[n+1]} \mathbf{H} \mathbf{R}_X^{[n+1]} \mathbf{H}^H (\Theta_r^{[n+1]})^H)$.
 - 6: $\rho^{[n+1]} = \rho^{[n]}$.
 - 7: **else**
 - 8: $\Upsilon^{[n+1]} = \Upsilon^{[n]}$, $\rho^{[n+1]} = c\rho^{[n]}$.
 - 9: **end if**
 - 10: $n = n + 1$.
 - 11: **until** the constraint violation $h(\mathcal{X})$ falls below a predefined threshold.
-

where $\mathcal{X} \triangleq \{\mathbf{U}, \mathbf{P}, \mathbf{R}_S, \mathbf{F}, \boldsymbol{\theta}_t, \boldsymbol{\theta}_r\}$ represents all the optimization variables and the entries of the matrix in the left-hand side of constant (23c) are given by

$$\mathbf{J}_{\phi\phi}(\mathbf{F}) = \frac{2|\alpha|^2 L}{\sigma_s^2} \text{Re} \left(\begin{bmatrix} \dot{\mathbf{B}}_{\phi_h} \mathbf{F} \dot{\mathbf{B}}_{\phi_h}^H & \dot{\mathbf{B}}_{\phi_h} \mathbf{F} \dot{\mathbf{B}}_{\phi_v}^H \\ \dot{\mathbf{B}}_{\phi_v} \mathbf{F} \dot{\mathbf{B}}_{\phi_h}^H & \dot{\mathbf{B}}_{\phi_v} \mathbf{F} \dot{\mathbf{B}}_{\phi_v}^H \end{bmatrix} \right), \quad (24)$$

$$\mathbf{J}_{\phi\tilde{\alpha}}(\mathbf{F}) = \frac{2L}{\sigma_s^2} \text{Re} \left(\begin{bmatrix} \alpha^* \text{tr}(\mathbf{B} \mathbf{F} \dot{\mathbf{B}}_{\phi_h}^H) \\ \alpha^* \text{tr}(\mathbf{B} \mathbf{F} \dot{\mathbf{B}}_{\phi_v}^H) \end{bmatrix} [1, j] \right), \quad (25)$$

$$\mathbf{J}_{\tilde{\alpha}\tilde{\alpha}}(\mathbf{F}) = \frac{2L}{\sigma_s^2} \mathbf{I}_2 \text{tr}(\mathbf{B} \mathbf{F} \mathbf{B}^H). \quad (26)$$

By introducing the Lagrangian dual variable $\Upsilon \in \mathbb{C}^{N \times N}$ for the equality constraints (23b) and the penalty parameter ρ , the following AL problem of (23) can be obtained:

$$\mathcal{P}_{\text{AL}}(\rho, \Upsilon) : \min_{\mathcal{X}} \quad \text{tr}(\mathbf{U}^{-1}) + P_{\rho}(\mathcal{X}, \Upsilon) \quad (27a)$$

$$\text{s.t.} \quad (21c) - (21f), (23c), \quad (27b)$$

where

$$P_{\rho}(\mathcal{X}, \Upsilon) = \frac{1}{2\rho} \|\mathbf{F} - \Theta_r \mathbf{H} \mathbf{R}_X \mathbf{H}^H \Theta_r^H + \rho \Upsilon\|^2. \quad (28)$$

According to [30], the PDD-based algorithm for solving \mathcal{P} is summarized in Algorithm 1, where $h(\mathcal{X})$ is the constraint violation function defined as

$$h(\mathcal{X}) = \|\mathbf{F} - \Theta_r \mathbf{H} \mathbf{R}_X \mathbf{H}^H \Theta_r^H\|_{\infty} \quad (29)$$

Moreover, $\{\eta^{[n]}\}_{n=1}^{\infty}$ is a sequence that converges to zero, which can be set empirically. In this paper, we set $\eta^{[n]} = 0.99h(\mathcal{X}^{[n-1]})$. It can be observed that when ρ is sufficiently small, the penalty term $P_{\rho}(\mathcal{X})$ and the constraint violation $h(\mathcal{X})$ will reduce to zero. In other words, the equality constraint (23b) is satisfied. The detailed discussion of the convergence and optimality

of the PDD framework can be found in [30].

C. Proposed BCD Algorithm for Solving AL Problem (27)

Now we turn our attention to solving the AL problem (27). Specifically, we divide \mathcal{X} into two blocks, namely $\{\mathbf{U}, \mathbf{F}, \mathbf{P}, \mathbf{R}_S\}$ and $\{\boldsymbol{\theta}_t, \boldsymbol{\theta}_r\}$. Then, the BCD algorithm is invoked to solve each block by fixing another block, which leads to the following two subproblems.

1) *Subproblem w.r.t. $\{\mathbf{U}, \mathbf{F}, \mathbf{P}, \mathbf{R}_S\}$* : The subproblem with respect to $\{\mathbf{U}, \mathbf{F}, \mathbf{P}, \mathbf{R}_S\}$ is

$$\min_{\mathbf{U}, \mathbf{F}, \mathbf{P}, \mathbf{R}_S} \quad \text{tr}(\mathbf{U}^{-1}) + \frac{1}{2\rho} \|\mathbf{F} - \boldsymbol{\Theta}_r \mathbf{H} \mathbf{R}_X \mathbf{H}^H \boldsymbol{\Theta}_r^H + \rho \boldsymbol{\Upsilon}\|^2 \quad (30a)$$

$$\text{s.t.} \quad \begin{bmatrix} \mathbf{J}_{\phi\phi}(\mathbf{F}) - \mathbf{U} & \mathbf{J}_{\phi\tilde{\alpha}}(\mathbf{F}) \\ \mathbf{J}_{\phi\tilde{\alpha}}^T(\mathbf{F}) & \mathbf{J}_{\tilde{\alpha}\tilde{\alpha}}(\mathbf{F}) \end{bmatrix} \succeq 0, \quad (30b)$$

$$\frac{1}{\Gamma} |\tilde{\mathbf{h}}_k^H \mathbf{p}_k|^2 \geq \sum_{i=1, i \neq k}^K |\tilde{\mathbf{h}}_k^H \mathbf{p}_i|^2 + \tilde{\mathbf{h}}_k^H \mathbf{R}_S \tilde{\mathbf{h}}_k + \sigma^2, \forall k \in \mathcal{K}, \quad (30c)$$

$$\text{tr}(\mathbf{P} \mathbf{P}^H + \mathbf{R}_S) \leq P, \mathbf{R}_S \succeq 0, \quad (30d)$$

where $\tilde{\mathbf{h}}_k^H = \mathbf{h}_k^H \boldsymbol{\Theta}_t \mathbf{H}$ denotes the effective channel for user k . Constraint (30c) is transformed from the communication SINR constraint (21c). Although problem (30) is apparently non-convex due to the constraint (30c), we now show that the global optimum of it can be obtained via semidefinite relaxation (SDP) technique.

Lemma 1. Given $\mathbf{P} = [\mathbf{p}_1, \dots, \mathbf{p}_K]^T$, there exists \mathbf{R}_X and \mathbf{R}_S that satisfy $\mathbf{R}_X = \mathbf{P} \mathbf{P}^H + \mathbf{R}_S$ if and only if

$$\mathbf{P} \mathbf{P}^H = \sum_{k \in \mathcal{K}} \mathbf{p}_k \mathbf{p}_k^H \preceq \mathbf{R}_X. \quad (31)$$

Proof. The necessity and sufficiency of this condition can be readily proved. ■

Applying Lemma 1 and defining the auxiliary variables $\mathbf{P}_k = \mathbf{p}_k \mathbf{p}_k^H, \forall k \in \mathcal{K}$ that satisfy $\text{rank}(\mathbf{P}_k) = 1$, we can formulate the SDR problem of (30) as follows:

$$\min_{\mathbf{U}, \mathbf{F}, \{\mathbf{P}_k\}, \mathbf{R}_X} \quad \text{tr}(\mathbf{U}^{-1}) + \frac{1}{2\rho} \|\mathbf{F} - \boldsymbol{\Theta}_r \mathbf{H} \mathbf{R}_X \mathbf{H}^H \boldsymbol{\Theta}_r^H + \rho \boldsymbol{\Upsilon}\|^2 \quad (32a)$$

$$\text{s.t.} \quad (1 + \frac{1}{\Gamma}) \tilde{\mathbf{h}}_k^H \mathbf{P}_k \tilde{\mathbf{h}}_k \geq \tilde{\mathbf{h}}_k^H \mathbf{R}_X \tilde{\mathbf{h}}_k + \sigma^2, \forall k \in \mathcal{K}, \quad (32b)$$

$$\text{tr}(\mathbf{R}_X) \leq P, \sum_{k \in \mathcal{K}} \mathbf{P}_k \preceq \mathbf{R}_X, (30b), \quad (32c)$$

where the non-convex rank-one constraints of $\mathbf{P}_k, \forall k \in \mathcal{K}$ are relaxed. It is not difficult to observe that problem (32) is convex semidefinite programming (SDP), the global optimum of which can be efficiently obtained by the existing convex optimization solvers. However, since the rank-one

constraints are omitted, the global optimum of problem (32) may have a higher rank, which is not a solution to the original non-convex problem (30). However, in the following proposition, we show that the rank-one global optimum of problem (30) can always be constructed from an arbitrary global optimum of problem (32).

Proposition 2. Given an arbitrary global optimum $\tilde{\mathbf{R}}_X, \{\tilde{\mathbf{P}}_k\}$ of problem (32), the following solution is a global optimum of problem (30):

$$\hat{\mathbf{R}}_X = \tilde{\mathbf{R}}_X, \quad \hat{\mathbf{p}}_k = (\tilde{\mathbf{h}}_k^H \tilde{\mathbf{P}}_k \tilde{\mathbf{h}}_k)^{-1/2} \tilde{\mathbf{P}}_k \tilde{\mathbf{h}}_k. \quad (33)$$

Proof. Please refer to [8, Theorem 1] ■

According to Proposition 2, a global optimum of problem (30) can be obtained by solving problem (32). Then, the optimal \mathbf{R}_S can be calculated as

$$\hat{\mathbf{R}}_S = \hat{\mathbf{R}}_X - \sum_{k \in \mathcal{K}} \hat{\mathbf{p}}_k \hat{\mathbf{p}}_k^H. \quad (34)$$

2) *Subproblem w.r.t. $\{\boldsymbol{\theta}_t, \boldsymbol{\theta}_r\}$:* The subproblem with respect to $\{\boldsymbol{\theta}_t, \boldsymbol{\theta}_r\}$ is given by

$$\min_{\boldsymbol{\theta}_t, \boldsymbol{\theta}_r} \|\mathbf{F} - \boldsymbol{\Theta}_r \mathbf{H} \mathbf{R}_X \mathbf{H}^H \boldsymbol{\Theta}_r^H + \rho \boldsymbol{\Upsilon}\|^2 \quad (35a)$$

$$\text{s.t.} \quad \gamma_k \geq \Gamma, \forall k \in \mathcal{K}, \quad (35b)$$

$$\beta_{t,n}^2 + \beta_{r,n}^2 \leq 1, 0 \leq \beta_{t,n}, \beta_{r,n} \leq 1, \forall n \in \mathcal{N}. \quad (35c)$$

To facilitate the optimization of $\boldsymbol{\theta}_t$ and $\boldsymbol{\theta}_r$, we first transform the objective function and the communication SINR γ_k to the more trackable forms. In particular, we define $\tilde{\mathbf{R}}_X = \mathbf{H} \mathbf{R}_X \mathbf{H}^H$, the eigenvalue decomposition of which is given by

$$\tilde{\mathbf{R}}_X = \sum_{k=1}^R \zeta_k \mathbf{v}_k \mathbf{v}_k^H = \sum_{i=1}^R \tilde{\mathbf{v}}_i \tilde{\mathbf{v}}_i^H, \quad (36)$$

where $\tilde{\mathbf{v}}_k = \sqrt{\zeta_k} \mathbf{v}_k$ with ζ_k and \mathbf{v}_k denoting the eigenvalue and the corresponding eigenvector, respectively, and R denotes the rank of matrix $\tilde{\mathbf{R}}_X$. Denoting $\tilde{\mathbf{F}}_{\mathbf{r}} = \mathbf{F} + \rho \boldsymbol{\Upsilon}$, the objective function can be reformulated as

$$\|\mathbf{F} - \sum_{i=1}^R \boldsymbol{\Theta}_r \tilde{\mathbf{v}}_i \tilde{\mathbf{v}}_i^H \boldsymbol{\Theta}_r^H + \rho \boldsymbol{\Upsilon}\|^2 = \|\tilde{\mathbf{F}} - \sum_{k=1}^R \text{diag}(\tilde{\mathbf{v}}_k) \boldsymbol{\theta}_r \boldsymbol{\theta}_r^H \text{diag}(\tilde{\mathbf{v}}_k)^H\|^2. \quad (37)$$

Next, denoting $\mathbf{a}_{k,i} = \text{diag}(\mathbf{h}_k^H) \mathbf{H} \mathbf{p}_i$ and $\mathbf{A}_k = \text{diag}(\mathbf{h}_k^H) \mathbf{H} \mathbf{R}_S \mathbf{H}^H \text{diag}(\mathbf{h}_k)$, the communication SINR $\gamma_k, \forall k \in \mathcal{K}$ can be reformulated as

$$\gamma_k = \frac{|\boldsymbol{\theta}_t^T \mathbf{a}_{k,k}|^2}{\sum_{i=1, i \neq k}^K |\boldsymbol{\theta}_t^T \mathbf{a}_{k,i}|^2 + \boldsymbol{\theta}_t^T \mathbf{A}_k \boldsymbol{\theta}_t^* + \sigma^2}. \quad (38)$$

As a consequence, problem (35) can be rewritten as

$$\min_{\tilde{\boldsymbol{\theta}}_t, \tilde{\boldsymbol{\theta}}_r} \left\| \tilde{\mathbf{F}} - \sum_{k=1}^R \tilde{\mathbf{V}}_k \boldsymbol{\theta}_r \boldsymbol{\theta}_r^H \tilde{\mathbf{V}}_k^H \right\|^2 \quad (39a)$$

$$\text{s.t.} \quad \frac{1}{\Gamma} |\boldsymbol{\theta}_t^T \mathbf{a}_{k,k}|^2 \geq \sum_{i=1, i \neq k}^K |\boldsymbol{\theta}_t^T \mathbf{a}_{k,i}|^2 + \boldsymbol{\theta}_t^T \mathbf{A}_k \boldsymbol{\theta}_t^* + \sigma^2, \forall k \in \mathcal{K}, \quad (39b)$$

$$|[\hat{\boldsymbol{\theta}}_t]_n|^2 + |[\hat{\boldsymbol{\theta}}_r]_n|^2 = 1, \forall n \in \mathcal{N}. \quad (39c)$$

Observing that the objective function and all the constraints of problem (39) are in quadratic form, we still exploit the SDR technique to approximately solve it efficiently. In particular, by defining the auxiliary variables $\mathbf{Q}_i = \boldsymbol{\theta}_i \boldsymbol{\theta}_i^H, \forall i \in \{t, r\}$, which satisfies $\mathbf{Q}_i \succeq 0$ and $\text{rank}(\mathbf{Q}_i) = 1$, the SDR problem of (39) is given by

$$\min_{\mathbf{Q}_t, \mathbf{Q}_r} \left\| \tilde{\mathbf{F}} - \sum_{k=1}^R \tilde{\mathbf{V}}_k \mathbf{Q}_r \tilde{\mathbf{V}}_k^H \right\|^2 \quad (40a)$$

$$\text{s.t.} \quad \frac{1}{\Gamma} \text{tr}(\mathbf{a}_{k,k} \mathbf{a}_{k,k}^H \mathbf{Q}_t^*) \geq \sum_{i=1, i \neq k}^K \text{tr}(\mathbf{a}_{k,i} \mathbf{a}_{k,i}^H \mathbf{Q}_t^*) + \text{tr}(\mathbf{A}_k \mathbf{Q}_t^*) + \sigma_k^2, \forall k \in \mathcal{K}, \quad (40b)$$

$$[\mathbf{Q}_t]_{n,n} + [\mathbf{Q}_r]_{n,n} = 1, \forall n \in \mathcal{N}, \quad (40c)$$

$$\mathbf{Q}_t \succeq 0, \mathbf{Q}_r \succeq 0, \quad (40d)$$

which is a convex SDP. The global optimum of it can be efficiently obtained via the existing convex optimization solvers. While the SDR may result in the solution with the general rank, the eigenvalue decomposition or Gaussian randomization [31] can be applied to construct a feasible rank-one solution to problem (39). Note that sufficiently number of Gaussian randomization can achieve at least $\frac{\pi}{4}$ -approximation of the optimal objective value of problem (39). However, the slight performance loss caused by constructing the rank-one solution cannot theoretically guarantee the monotonicity of the objective value during the iterations of BCD. In this case, the penalty-based alternating minimization (AltMin) algorithm proposed in [17] with the provable convergence to the stationary point can be exploited, where the rank-one constraints are transformed as a penalty term in the objective function. Nevertheless, it is worth mentioning that the eigenvalue decomposition or Gaussian randomization can generally guarantee the convergence in practice.

The overall BCD algorithm for solving problem (27) is summarized in Algorithm 2. Basically, the stationary points can be obtained at each step of BCD when the AltMin algorithm is exploited. Therefore, this algorithm is guaranteed to converge to a stationary point of problem (27) in

Algorithm 2 BCD algorithm for solving problem (27).

- 1: Initialize feasible \mathcal{X} .
 - 2: **repeat**
 - 3: update $\{\mathbf{U}, \mathbf{F}, \mathbf{P}, \mathbf{R}_S\}$ by solving problem (32).
 - 4: update $\{\boldsymbol{\theta}_t, \boldsymbol{\theta}_r\}$ by solving problem (40).
 - 5: **until** the fractional reduction of the objective value falls below a predefined threshold.
-

polynomial time [32]. The main complexity of Algorithm 2 arises from solving problem (32) and (40). Since both of them are QSDP, given the solution accuracy ϵ , the corresponding complexity via the interior-point method is in order of $\mathcal{O}((K^{6.5}M^{6.5} + N^{6.5})\log(1/\epsilon))$ and $\mathcal{O}((K + N)^{6.5}N^{6.5}\log(1/\epsilon))$, respectively [8], [33].

IV. CRB OPTIMIZATION DESIGN WITH COUPLED T&R PHASE-SHIFT

In this section, we turn our attention to the CRB optimization with coupled T&R phase-shift. Following a similar path in Section IV, the PDD framework is also invoked. Regarding the coupled T&R phase-shift constraints, a low-complexity AO algorithm is proposed, where the optimal amplitudes and phase-shifts of SATRS coefficients are obtained in closed-form.

A. Problem Formulation

According to Proposition 1, the optimization problem for minimizing $\text{CRB}(\phi)$ with the coupled phase shift can be formulated as follows:

$$\tilde{\mathcal{P}} : \min_{\mathbf{U}, \mathbf{P}, \mathbf{R}_S, \boldsymbol{\theta}_r, \boldsymbol{\theta}_t} \text{tr}(\mathbf{U}^{-1}), \quad (41a)$$

$$\text{s.t. } \beta_{t,n}\beta_{r,n}\cos(\varphi_{t,n} - \varphi_{r,n}) = 0, \forall n \in \mathcal{N}, \quad (41b)$$

$$(21b) - (21f), \quad (41c)$$

where constraint (41b) characterize the amplitude and phase-shift relationships between TCs and RCs. Note that, the elements of the STAR-RIS is preferred to work in the simultaneously transmitting and reflecting mode. Thus, it generally holds that $\beta_{t,n} \neq 0$ and $\beta_{r,n} \neq 0$, leading to a simplified form of the coupled T&R phase-shift constraint (41b):

$$|\varphi_{t,n} - \varphi_{r,n}| = \frac{1}{2}\pi \text{ or } \frac{3}{2}\pi. \quad (42)$$

The coupled T&R phase-shift model imposed in (41b) makes the problem even more complex compared to the independent phase-shift model. As a consequence, in the following subsections, we develop another efficient PDD-based algorithm to solve the coupled T&R phase-shift constraints.

B. PDD Framework for Solving Problem $\tilde{\mathcal{P}}$

In Section III, we have proposed a PDD-based algorithm for the independent T&R phase-shift model. In this case, we aim to obtain an equivalent form of problem (41) where the coupled T&R phased-shift is relaxed to the independent one. Toward this idea, apart from $\mathbf{F} = \mathbf{\Theta}_r \mathbf{H} \mathbf{R}_X \mathbf{H}^H \mathbf{\Theta}_r^H$, we define another set of auxiliary variables:

$$\tilde{\boldsymbol{\theta}}_i = \boldsymbol{\theta}_i, \forall i \in \{t, r\}, \quad (43)$$

where $\tilde{\boldsymbol{\theta}}_i = [\tilde{\beta}_{i,1} e^{j\tilde{\varphi}_{i,1}}, \dots, \tilde{\beta}_{i,N} e^{j\tilde{\varphi}_{i,N}}]^T, \forall i \in \{t, r\}$. Then, $\tilde{\mathcal{P}}$ can be reformulated as

$$\min_{\tilde{\mathcal{X}}} \quad \text{tr}(\mathbf{U}^{-1}) \quad (44a)$$

$$\text{s.t.} \quad \tilde{\boldsymbol{\theta}}_r = \boldsymbol{\theta}_r, \tilde{\boldsymbol{\theta}}_t = \boldsymbol{\theta}_t, \quad (44b)$$

$$\tilde{\beta}_{t,n}^2 + \tilde{\beta}_{r,n}^2 = 1, 0 \leq \tilde{\beta}_{t,n}, \tilde{\beta}_{r,n} \leq 1, \forall n \in \mathcal{N}, \quad (44c)$$

$$|\tilde{\varphi}_{t,n} - \tilde{\varphi}_{r,n}| = \frac{1}{2}\pi \text{ or } \frac{3}{2}\pi, \forall n \in \mathcal{N}, \quad (44d)$$

$$\beta_{t,n}^2 + \beta_{r,n}^2 = 1, 0 \leq \beta_{t,n}, \beta_{r,n} \leq 1, \forall n \in \mathcal{N}, \quad (44e)$$

$$(21c) - (21f), (23b), (23c) \quad (44f)$$

where $\tilde{\mathcal{X}} \triangleq \{\mathbf{U}, \mathbf{P}, \mathbf{R}_S, \mathbf{F}, \boldsymbol{\theta}_t, \boldsymbol{\theta}_r, \tilde{\boldsymbol{\theta}}_t, \tilde{\boldsymbol{\theta}}_r\}$ represents all the optimization variables. Note that in problem (44), the phase-shift constraints of the original optimization variables $\boldsymbol{\theta}_t$ and $\boldsymbol{\theta}_r$ have been relaxed to be independent, and the coupled T&R phase-shift constraints are only related to the auxiliary variables $\tilde{\boldsymbol{\theta}}_t$ and $\tilde{\boldsymbol{\theta}}_r$. By introducing the Lagrangian dual variable $\boldsymbol{\lambda}_i \in \mathbb{C}^{N \times 1}, \forall i \in \{t, r\}$ for the additional equality constraints (44b) and the penalty parameter ρ , the following AL problem of (44) can be obtained:

$$\tilde{\mathcal{P}}_{\text{AL}}(\rho, \boldsymbol{\Upsilon}, \boldsymbol{\lambda}_i) : \min_{\tilde{\mathcal{X}}} \quad \text{tr}(\mathbf{U}^{-1}) + \tilde{P}_\rho(\tilde{\mathcal{X}}, \boldsymbol{\Upsilon}, \boldsymbol{\lambda}_i) \quad (45a)$$

$$\text{s.t.} \quad (21c) - (21f), (23b), (23c), (44b) - (44e), \quad (45b)$$

where

$$\tilde{P}_\rho(\tilde{\mathcal{X}}, \boldsymbol{\Upsilon}, \boldsymbol{\lambda}_i) = \frac{1}{2\rho} \left(\|\mathbf{F} - \mathbf{\Theta}_r \mathbf{H} \mathbf{R}_X \mathbf{H}^H \mathbf{\Theta}_r^H + \rho \boldsymbol{\Upsilon}\|^2 + \sum_{i \in \{t, r\}} \|\tilde{\boldsymbol{\theta}}_i - \boldsymbol{\theta}_i + \rho \boldsymbol{\lambda}_i\|^2 \right) \quad (46)$$

Thus, the PDD-based algorithm for solving $\tilde{\mathcal{P}}$ is summarized in Algorithm 3 and the constraint violation function is defined as

$$\tilde{h}(\tilde{\mathcal{X}}) = \max \left\{ \|\mathbf{F} - \mathbf{\Theta}_r \mathbf{H} \mathbf{R}_X \mathbf{H}^H \mathbf{\Theta}_r^H\|_\infty, \|\tilde{\boldsymbol{\theta}}_t - \boldsymbol{\theta}_t\|_\infty, \|\tilde{\boldsymbol{\theta}}_r - \boldsymbol{\theta}_r\|_\infty \right\}. \quad (47)$$

Algorithm 3 PDD-based algorithm for solving problem $\tilde{\mathcal{P}}$.

- 1: Initialize feasible $\tilde{\mathcal{X}}^{[0]}$, $\Upsilon^{[0]}$, $\lambda_i^{[0]}$, $\forall i \in \{t, r\}$, $\rho^{[0]} \geq 0$, and set $0 < c < 1$, $n = 1$.
 - 2: **repeat**
 - 3: $\tilde{\mathcal{X}}^{[n+1]} = \text{optimize} \left(\tilde{\mathcal{P}}_{\text{AL}}(\rho^{[n]}, \Upsilon^{[n]}, \lambda_i^{[n]}) \right)$
 - 4: **if** $h(\tilde{\mathcal{X}}^{[n+1]}) \leq \eta^{[n]}$ **then**
 - 5: $\Upsilon^{[n+1]} = \Upsilon^{[n]} + \frac{1}{\rho}(\mathbf{F}^{[n+1]} - \Theta_r^{[n+1]} \mathbf{H} \mathbf{R}_X^{[n+1]} \mathbf{H}^H (\Theta_r^{[n+1]})^H)$.
 - 6: $\lambda_i^{[n+1]} = \lambda_i^{[n]} + \frac{1}{\rho}(\tilde{\theta}_i^{[n+1]} - \theta_i^{[n+1]})$, $\forall i \in \{t, r\}$.
 - 7: $\rho^{[n+1]} = \rho^{[n]}$.
 - 8: **else**
 - 9: $\Upsilon^{[n+1]} = \Upsilon^{[n]}$, $\lambda_i^{[n+1]} = \lambda_i^{[n]}$, $\forall i \in \{t, r\}$.
 - 10: $\rho^{[n+1]} = c\rho^{[n]}$.
 - 11: **end if**
 - 12: $n = n + 1$.
 - 13: **until** the constraint violation $\tilde{h}(\tilde{\mathcal{X}})$ falls below a predefined threshold.
-

C. Proposed BCD Algorithm for Solving AL Problem (45)

Similar as that in Section III-C, the BCD is exploited to solve problem (45), where the set of optimization variables $\tilde{\mathcal{X}}$ is divided into three blocks, namely $\{\mathbf{U}, \mathbf{F}, \mathbf{P}, \mathbf{R}_S\}$, $\{\theta_t, \theta_r\}$, and $\{\tilde{\theta}_t, \tilde{\theta}_r\}$. The solutions of the corresponding subproblems are given as follows.

1) *Subproblem w.r.t. $\{\mathbf{U}, \mathbf{F}, \mathbf{P}, \mathbf{R}_S\}$* : The subproblem with respect to $\{\mathbf{U}, \mathbf{F}, \mathbf{P}, \mathbf{R}_S\}$ for the coupled phase shift model is the same as that for the independent phase-shift model. Thus, it can be solved following the same path in Section III-C1.

2) *Subproblem w.r.t. $\{\theta_t, \theta_r\}$* : The subproblem with respect to $\{\theta_t, \theta_r\}$ can be optimized with the relaxed amplitude and phase-shift constraint, which is given by

$$\min_{\theta_r, \theta_t} \quad \|\mathbf{F} - \Theta_r \mathbf{H} \mathbf{R}_X \mathbf{H}^H \Theta_r^H + \rho \Upsilon\|^2 + \sum_{i \in \{t, r\}} \|\tilde{\theta}_i - \theta_i + \rho \lambda_i\|^2 \quad (48a)$$

$$\text{s.t.} \quad \gamma_k \geq \Gamma, \quad (48b)$$

$$\beta_{t,n}^2 + \beta_{r,n}^2 = 1, 0 \leq \beta_{t,n}, \beta_{r,n} \leq 1, \forall n \in \mathcal{N}. \quad (48c)$$

Then, denoting $\tilde{\mathbf{F}}_\Upsilon = \mathbf{F} + \rho \Upsilon$, and $\tilde{\theta}_{\lambda,i} = \tilde{\theta}_i + \rho \lambda_i$, $\forall i \in \{t, r\}$, the objective function can be reformulated as

$$\begin{aligned} & \|\tilde{\mathbf{F}} - \sum_{k=1}^{R_1} \text{diag}(\tilde{\mathbf{v}}_k) \theta_r \theta_r^H \text{diag}(\tilde{\mathbf{v}}_k)^H\|^2 + \sum_{i \in \{t, r\}} \|\tilde{\theta}_{\lambda,i} - \theta_i\|^2 \\ &= \|\tilde{\mathbf{F}} - \sum_{k=1}^{R_1} \tilde{\mathbf{V}}_k \hat{\theta}_r \hat{\theta}_r^H \tilde{\mathbf{V}}_k^H\|^2 + \sum_{i \in \{t, r\}} (\hat{\theta}_i^H \mathbf{C}_i \hat{\theta}_i + \tilde{\theta}_{\lambda,i}^H \tilde{\theta}_{\lambda,i}), \end{aligned} \quad (49)$$

where

$$\tilde{\mathbf{V}}_k = \begin{bmatrix} \text{diag}(\tilde{\mathbf{v}}_k) & \mathbf{0}_N \end{bmatrix}, \mathbf{C}_i = \begin{bmatrix} \mathbf{I}_N & -\tilde{\boldsymbol{\theta}}_{\lambda,i} \\ -\tilde{\boldsymbol{\theta}}_{\lambda,i}^H & 0 \end{bmatrix}, \hat{\boldsymbol{\theta}}_i = \begin{bmatrix} \mu_i \boldsymbol{\theta}_i \\ \mu_i \end{bmatrix}, \quad (50)$$

and $|\mu_i|^2 = 1$. Next, the communication SINR $\gamma_k, \forall k \in \mathcal{K}$ can be reformulated as

$$\gamma_k = \frac{|\boldsymbol{\theta}_t^T \mathbf{a}_{k,k}|^2}{\sum_{i=1, i \neq k}^K |\boldsymbol{\theta}_t^T \mathbf{a}_{k,i}|^2 + \boldsymbol{\theta}_t^T \mathbf{A}_k \boldsymbol{\theta}_t^* + \sigma^2} = \frac{\hat{\boldsymbol{\theta}}_t^T \mathbf{D}_{k,1} \hat{\boldsymbol{\theta}}_t}{\hat{\boldsymbol{\theta}}_t^T \mathbf{D}_{k,2} \hat{\boldsymbol{\theta}}_t + \sigma_k^2}, \quad (51)$$

where

$$\mathbf{D}_{k,1} = \begin{bmatrix} \mathbf{a}_{k,k} \mathbf{a}_{k,k}^H & \mathbf{0}_N \\ \mathbf{0}_N^T & 0 \end{bmatrix}, \mathbf{D}_{k,2} = \begin{bmatrix} \sum_{i=1, i \neq k}^K \mathbf{a}_{k,i} \mathbf{a}_{k,i}^H + \mathbf{A}_k & \mathbf{0}_N \\ \mathbf{0}_N^T & 0 \end{bmatrix} \quad (52)$$

It can be observed that the objective function and all the constraints of problem (48) have been transformed into quadratic form. Thus, we also exploit the SDR technique to approximately solve it. In particular, by defining the auxiliary variables $\hat{\mathbf{Q}}_i = \hat{\boldsymbol{\theta}}_i \hat{\boldsymbol{\theta}}_i^H, \forall i \in \{t, r\}$, which satisfies $\hat{\mathbf{Q}}_i \succeq 0$ and $\text{rank}(\hat{\mathbf{Q}}_i) = 1$, the SDR problem of (48) is given by

$$\min_{\hat{\boldsymbol{\theta}}_t, \hat{\boldsymbol{\theta}}_r} \quad \|\tilde{\mathbf{F}} - \sum_{k=1}^{R_1} \tilde{\mathbf{V}}_k \hat{\mathbf{Q}}_t \tilde{\mathbf{V}}_k^H\|^2 + \sum_{i \in \{t, r\}} (\text{tr}(\mathbf{C}_i \hat{\mathbf{Q}}_i) + \tilde{\boldsymbol{\theta}}_{\lambda,i}^H \tilde{\boldsymbol{\theta}}_{\lambda,i}) \quad (53a)$$

$$\text{s.t.} \quad \frac{1}{\Gamma} \text{tr}(\mathbf{D}_{k,1} \hat{\mathbf{Q}}_t^*) \geq \text{tr}(\mathbf{D}_{k,2} \hat{\mathbf{Q}}_t^*) + \sigma_k^2, \forall k \in \mathcal{K}, \quad (53b)$$

$$[\hat{\mathbf{Q}}_t]_{n,n} + [\hat{\mathbf{Q}}_r]_{n,n} = 1, \forall n \in \mathcal{N}, \quad (53c)$$

$$[\hat{\mathbf{Q}}_t]_{N+1, N+1} = [\hat{\mathbf{Q}}_r]_{N+1, N+1} = 1, \quad (53d)$$

$$\hat{\mathbf{Q}}_t \succeq 0, \hat{\mathbf{Q}}_r \succeq 0, \quad (53e)$$

which is a convex SDP. Let $\hat{\boldsymbol{\theta}}_i^{\text{opt}}, \forall i \in \{t, r\}$ denotes the approximated rank-one solution. Then, the corresponding solution of problem (48) is given by

$$\boldsymbol{\theta}_i^{\text{opt}} = \frac{1}{[\hat{\boldsymbol{\theta}}_i^{\text{opt}}]_{N+1}} [\hat{\boldsymbol{\theta}}_i^{\text{opt}}]_{1:N}, \forall i \in \{t, r\}. \quad (54)$$

Similarly, the penalty-based AltMin method in [17] can be employed to guarantee the theoretical convergence of the BCD.

3) *Subproblem w.r.t. $\{\tilde{\boldsymbol{\theta}}_t, \tilde{\boldsymbol{\theta}}_r\}$* : The optimization variable $\{\tilde{\boldsymbol{\theta}}_t, \tilde{\boldsymbol{\theta}}_r\}$ only appears in the penalty term in the objective function with the coupled amplitude and phase-shift constraints. Thus, the subproblem with respect to $\{\tilde{\boldsymbol{\theta}}_t, \tilde{\boldsymbol{\theta}}_r\}$ is given by

$$\min_{\tilde{\boldsymbol{\theta}}_t, \tilde{\boldsymbol{\theta}}_r} \quad \|\tilde{\boldsymbol{\theta}}_t - \boldsymbol{\theta}_t + \rho \boldsymbol{\lambda}_t\|^2 + \|\tilde{\boldsymbol{\theta}}_r - \boldsymbol{\theta}_r + \rho \boldsymbol{\lambda}_r\|^2 \quad (55a)$$

$$\text{s.t.} \quad \tilde{\beta}_{t,n}^2 + \tilde{\beta}_{r,n}^2 = 1, 0 \leq \tilde{\beta}_{t,n}, \tilde{\beta}_{r,n} \leq 1, \forall n \in \mathcal{N}, \quad (55b)$$

$$|\tilde{\varphi}_{t,n} - \tilde{\varphi}_{r,n}| = \frac{1}{2}\pi \text{ or } \frac{3}{2}\pi, \forall n \in \mathcal{N}. \quad (55c)$$

In this problem, both constraints are non-convex and the second constraint even requires a binary decision, which is challenging to solve. However, in the following, we show that the amplitude coefficients and the phase-shift coefficients can be optimized with the closed-form solution in an alternative manner. To this end, we reformulate $\tilde{\boldsymbol{\theta}}_i$ as

$$\tilde{\boldsymbol{\theta}}_i = \text{diag}(\tilde{\boldsymbol{\beta}}_i) \tilde{\mathbf{q}}_i, \forall i \in \{t, r\}, \quad (56)$$

where $\tilde{\boldsymbol{\beta}}_i = [\tilde{\beta}_{i,1}, \dots, \tilde{\beta}_{i,N}]^T$ and $\tilde{\mathbf{q}}_i = [e^{j\tilde{\varphi}_{i,1}}, \dots, e^{j\tilde{\varphi}_{i,N}}]$. By defining $\boldsymbol{\vartheta}_i = -\boldsymbol{\theta}_i + \rho \boldsymbol{\lambda}_i, \forall i \in \{t, r\}$, the objective function of (55) can be rewritten as

$$\begin{aligned} \sum_{i \in \{t, r\}} \|\tilde{\boldsymbol{\theta}}_i + \boldsymbol{\vartheta}_i\|^2 &= \sum_{i \in \{t, r\}} \|\text{diag}(\tilde{\boldsymbol{\beta}}_i) \tilde{\mathbf{q}}_i + \boldsymbol{\vartheta}_i\|^2 \\ &= \sum_{i \in \{t, r\}} \tilde{\mathbf{q}}_i^H \text{diag}(\tilde{\boldsymbol{\beta}}_i) \text{diag}(\tilde{\boldsymbol{\beta}}_i) \tilde{\mathbf{q}}_i + \sum_{i \in \{t, r\}} \boldsymbol{\vartheta}_i^H \boldsymbol{\vartheta}_i + \sum_{i \in \{t, r\}} 2\text{Re}(\boldsymbol{\vartheta}_i^H \text{diag}(\tilde{\boldsymbol{\beta}}_i) \tilde{\mathbf{q}}_i) \\ &\stackrel{(a)}{=} \sum_{i \in \{t, r\}} \sum_{n \in \mathcal{N}} \tilde{\beta}_{i,n}^2 + \sum_{i \in \{t, r\}} \boldsymbol{\vartheta}_i^H \boldsymbol{\vartheta}_i + \sum_{i \in \{t, r\}} 2\text{Re}(\boldsymbol{\vartheta}_i^H \text{diag}(\tilde{\boldsymbol{\beta}}_i) \tilde{\mathbf{q}}_i) \\ &\stackrel{(b)}{=} \underbrace{N + \sum_{i \in \{t, r\}} \boldsymbol{\vartheta}_i^H \boldsymbol{\vartheta}_i}_{\text{constant}} + \sum_{i \in \{t, r\}} 2\text{Re}(\boldsymbol{\vartheta}_i^H \text{diag}(\tilde{\boldsymbol{\beta}}_i) \tilde{\mathbf{q}}_i), \end{aligned} \quad (57)$$

where the equality (a) is due to the property $|\tilde{\mathbf{q}}_i|_n|^2 = |e^{j\tilde{\varphi}_{i,n}}|^2 = 1$, and the equality (b) is due to the property $\tilde{\beta}_{t,n}^2 + \tilde{\beta}_{r,n}^2 = 1$. By removing the constant in the objective function, problem (55) can be simplified as

$$\min_{\tilde{\boldsymbol{\beta}}_t, \tilde{\boldsymbol{\beta}}_r, \tilde{\mathbf{q}}_t, \tilde{\mathbf{q}}_r} \text{Re}(\boldsymbol{\vartheta}_t^H \text{diag}(\tilde{\boldsymbol{\beta}}_t) \tilde{\mathbf{q}}_t) + \text{Re}(\boldsymbol{\vartheta}_r^H \text{diag}(\tilde{\boldsymbol{\beta}}_r) \tilde{\mathbf{q}}_r) \quad (58a)$$

$$\text{s.t. } (55b), (55c). \quad (58b)$$

Proposition 3. (*Closed-form solution for coupled T&R phase-shift*) With the coupled T&R phase-shift constraint (55c), for any given $\tilde{\boldsymbol{\beta}}_t$ and $\tilde{\boldsymbol{\beta}}_r$, the optimal solution for the n -th entries $\tilde{q}_{t,n}, \tilde{q}_{r,n}$ of $\tilde{\mathbf{q}}_t, \tilde{\mathbf{q}}_r$ are chosen from the following two pairs of solutions

$$\begin{cases} \tilde{q}_{t,n} = e^{j(\pi - \angle \psi_n^+)}, \tilde{q}_{r,n} = e^{j(\frac{3}{2}\pi - \angle \psi_n^+)}, \\ \tilde{q}_{t,n} = e^{j(\pi - \angle \psi_n^-)}, \tilde{q}_{r,n} = e^{j(\frac{1}{2}\pi - \angle \psi_n^-)}, \end{cases} \quad (59)$$

where $\psi_n^+ = \tilde{\vartheta}_{t,n}^* + j\tilde{\vartheta}_{r,n}^*$ and $\psi_n^- = \tilde{\vartheta}_{t,n}^* - j\tilde{\vartheta}_{r,n}^*$, such that the value of $\text{Re}(\tilde{\vartheta}_{t,n}^* \tilde{q}_{t,n}) + \text{Re}(\tilde{\vartheta}_{r,n}^* \tilde{q}_{r,n})$ is minimized. Here, $\tilde{\vartheta}_{i,n}^*$ denotes the n -th entry of the vector $\tilde{\boldsymbol{\vartheta}}_i^H = \boldsymbol{\vartheta}_i^H \text{diag}(\tilde{\boldsymbol{\beta}}_i), \forall i \in \{t, r\}$.

Proof. Please refer to Appendix B. ■

Algorithm 4 AO algorithm for solving problem (55).

- 1: Initialize feasible $\tilde{\mathbf{q}}_t$, $\tilde{\mathbf{q}}_r$, $\tilde{\boldsymbol{\beta}}_t$, and $\tilde{\boldsymbol{\beta}}_r$.
 - 2: **repeat**
 - 3: update each entry of $\tilde{\mathbf{q}}_t$ and $\tilde{\mathbf{q}}_r$ by (59)
 - 4: update each entry of $\tilde{\boldsymbol{\beta}}_t$ and $\tilde{\boldsymbol{\beta}}_r$ by (60).
 - 5: **until** the fractional reduction of the objective value falls below a predefined threshold.
-

Algorithm 5 BCD algorithm for solving problem (45).

- 1: Initialize feasible $\tilde{\mathcal{X}}$ such that $\mathbf{F} = \boldsymbol{\Theta}_r \mathbf{H} \mathbf{R}_X \mathbf{H}^H \boldsymbol{\Theta}_r^H$ and $\tilde{\boldsymbol{\theta}}_i = \boldsymbol{\theta}_i, \forall i \in \{t, r\}$.
 - 2: **repeat**
 - 3: update $\{\mathbf{U}, \mathbf{F}, \mathbf{P}, \mathbf{R}_S\}$ by solving problem (32).
 - 4: update $\{\boldsymbol{\theta}_t, \boldsymbol{\theta}_r\}$ by solving problem (53).
 - 5: update $\{\tilde{\boldsymbol{\theta}}_t, \tilde{\boldsymbol{\theta}}_r\}$ by solving problem (55) using Algorithm 4.
 - 6: **until** the fractional reduction of the objective value falls below a predefined threshold.
-

Proposition 4. (*Closed-form solution for amplitude*) For any given $\tilde{\mathbf{q}}_t$ and $\tilde{\mathbf{q}}_r$, the optimal solution of the n -th entries $\tilde{\beta}_{t,n}$, $\tilde{\beta}_{r,n}$ of $\tilde{\boldsymbol{\beta}}_t$, $\tilde{\boldsymbol{\beta}}_r$ are given by

$$\tilde{\beta}_{t,n} = \sin \omega_n, \tilde{\beta}_{r,n} = \cos \omega_n, \quad (60)$$

$$\omega_n = \begin{cases} -\frac{1}{2}\pi - \psi_n, & \text{if } \psi_n \in [-\pi, -\frac{1}{2}\pi), \\ 0, & \text{if } \psi_n \in [-\frac{1}{2}\pi, \frac{1}{4}\pi), \\ \frac{1}{2}\pi, & \text{otherwise,} \end{cases} \quad (61)$$

where $\psi_n = \text{sgn}(b_n) \arccos(\frac{a_n}{\sqrt{a_n^2 + b_n^2}}) \in [-\pi, \pi]$, $a_n = |\check{\vartheta}_{t,n}^*| \cos(\angle \check{\vartheta}_{t,n}^*)$, $b_n = |\check{\vartheta}_{r,n}^*| \cos(\angle \check{\vartheta}_{r,n}^*)$, and $\check{\vartheta}_{i,n}^*$ is the n -th entry of the vector $\check{\boldsymbol{\vartheta}}_i^H = \boldsymbol{\vartheta}_i^H \text{diag}(\tilde{\mathbf{q}}_i), \forall i \in \{t, r\}$.

Proof. Please refer to Appendix C. ■

According to Proposition 3 and Proposition 4, by fixing the amplitude (phase-shift) coefficients, the phase-shift (amplitude) coefficients have the optimal closed-form solutions. Consequently, problem (55) can also be solved by invoking AO, the detail of which is given in Algorithm 4. Since the optimal solution is obtained at each step, the convergence of Algorithm 4 to the stationary points is also guaranteed [32].

The overall BCD algorithm for solving problem (45) is summarized in Algorithm 5. Similarly, when the AltMin method is adopted for optimizing the block $\{\boldsymbol{\theta}_t, \boldsymbol{\theta}_r\}$, the convergence of Algorithm 5 to the stationary point can be theoretically proved [32]. The complexity of this algorithm is summarized as follows. Firstly, the complexities of using the interior-point method to solve QSDP problem (32) and (53) are in order of $\mathcal{O}((K^{6.5}M^{6.5} + N^{6.5}) \log(1/\epsilon))$ and $\mathcal{O}((K +$

$N + 2)^{6.5}(N + 1)^{6.5} \log(1/\epsilon))$, respectively [8], [33]. Moreover, in Algorithm 4, the complexities of updating $\{\tilde{\mathbf{q}}_t, \tilde{\mathbf{q}}_r\}$ and $\{\tilde{\boldsymbol{\beta}}_t, \tilde{\boldsymbol{\beta}}_r\}$ are in order of $\mathcal{O}(4N)$ and $\mathcal{O}(2N)$, respectively.

V. NUMERICAL RESULTS

In this section, the simulation results are provided to verify the effectiveness of the proposed STARS-enabled ISAC system. The following parameter setup is assumed throughout our simulations unless otherwise specified. The ULAs of BS and sensor are assumed to have $M = 10$ and $N_S = 5$ elements with half-wavelength spacing. The UPA of STARS is assumed to have $N = 5 \times 2$ elements with half-wavelength spacing. The power budget at the BS is set as $P = 30\text{dBm}$. The BS is assumed to locate at $(30^\circ, 0^\circ)$ and 40m from the STARS. The communication users are randomly distributed within a range (20m, 50m) at the transmission side of STARS, and the sensing target is in the direction of $(120^\circ, 30^\circ)$ and with a distance of 30m at the reflection side of STARS. The channels \mathbf{H} and $\mathbf{h}_k, \forall k$ are assumed to obey the Rician channel model:

$$\mathbf{H} = \sqrt{\frac{1}{\Lambda_{BR}}} \left(\sqrt{\frac{\varepsilon}{1+\varepsilon}} \mathbf{H}^{\text{LoS}} + \sqrt{\frac{1}{1+\varepsilon}} \mathbf{H}^{\text{NLoS}} \right), \quad (62)$$

$$\mathbf{h}_k = \sqrt{\frac{1}{\Lambda_{RU}}} \left(\sqrt{\frac{\varepsilon}{1+\varepsilon}} \mathbf{h}_k^{\text{LoS}} + \sqrt{\frac{1}{1+\varepsilon}} \mathbf{h}_k^{\text{NLoS}} \right), \quad (63)$$

where Λ_{BR} and Λ_{RU} are the path loss following $\Lambda = \Lambda_0 + 20 \log_{10}(d)\text{dB}$ with $\Lambda_0 = 30\text{dB}$ denoting the path loss at the reference distance $d = 1\text{m}$. ε denotes the Rician factor, which is set as $\varepsilon = 1$. \mathbf{H}^{LoS} and $\mathbf{h}_k^{\text{LoS}}$ are the deterministic LoS component, and \mathbf{H}^{NLoS} and $\mathbf{h}_k^{\text{NLoS}}$ are the random non LoS component model as Rayleigh fading. The noise power at the sensor and communication users is set as -110dBm . Finally, the sensing dwell time is set as $L = 100$. To verify the efficiency of the proposed framework, we compared it with a baseline that employs one conventional reflecting-only RIS and one conventional transmitting-only RIS, both with $\frac{N}{2}$ elements and adjacent to each other at the same location as the STARS. This baseline is essentially a special case of STARS where the amplitudes of the TCs and RCs are fixed to $\boldsymbol{\beta}_t = [\mathbf{1}_{\frac{N}{2}}; \mathbf{0}_{\frac{N}{2}}]$ and $\boldsymbol{\beta}_r = [\mathbf{0}_{\frac{N}{2}}; \mathbf{1}_{\frac{N}{2}}]$. Therefore, the resultant optimization problem can also be solved by the proposed PDD-based algorithm. All the following numerical results are obtained by averaging over 50 random channel realizations unless otherwise specified.

A. Convergence Performance of the Proposed Algorithms

We firstly examine the overall convergence performance of the proposed algorithms over a random channel realization in Fig. 2 and Fig. 3. In particular, the initialization point of Algorithm 1 is randomly selected while that of Algorithm 3 is selected as the output of Algorithm 1. Note

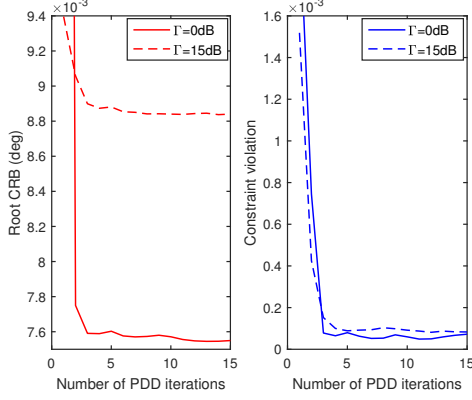


Fig. 2: The convergence behavior of Algorithm 1.

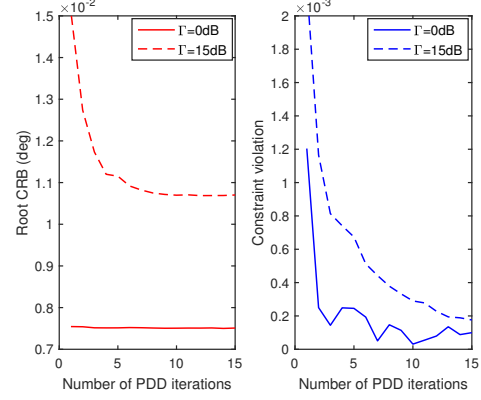


Fig. 3: The convergence behavior of Algorithm 3.

that the original unit of the root CRB is radian, which is difficult to match intuitively with the accuracy of the practical DOA estimates. Thus, we convert the unit of the root CRB from radian to degree. In terms of the root CRB and the constraint violation, it can be observed that they can converge well for both independent and coupled phase-shift models by using Algorithm 1 and Algorithm 3. Moreover, when the SINR threshold is low, namely $\Gamma = 0\text{dB}$, the Algorithm 3 almost converges at the first PDD iteration. This is because, with the low SINR threshold, the coupled phase-shift model is almost identical to the independent phase-shift model. Consequently, when Algorithm 3 is initialized as the output of Algorithm 1, the optimal solution is almost reached at the beginning. This phenomenon will be further explained in the following numerical results. Next, to verify the effectiveness of the proposed coupled phase-shift optimization framework, we examine the phase-shift difference $|\varphi_{t,n} - \varphi_{r,n}|$ of each STARS element as the iterations progress when $\Gamma = 15\text{dB}$. Fig. 4 illustrates that the convergence of phase-shift difference at the first iteration of Algorithm 3. We can see that the phase-shift difference of all the STARS elements converges to $\frac{\pi}{2}$ or $\frac{3\pi}{2}$, which verifies that the coupled phase-shift constraints can be achieved.

B. Root CRB Versus Communication SINR Threshold

In Fig. 5, we studied the achieved root CRB versus the communication SINR threshold considering different user numbers. As can be observed, there is a trade-off between the sensing and communication performance. This is because the higher communication performance requires more resources such as power and DoFs in the communication space, resulting in lower sensing performance. It can also be seen that independent of the phase shift model, STARS always outperforms conventional RIS in achieving a lower CRB. The conventional RIS almost becomes infeasible when $K = 6$ and $\Gamma > 6\text{dB}$. This is indeed expected since conventional RIS utilizes a

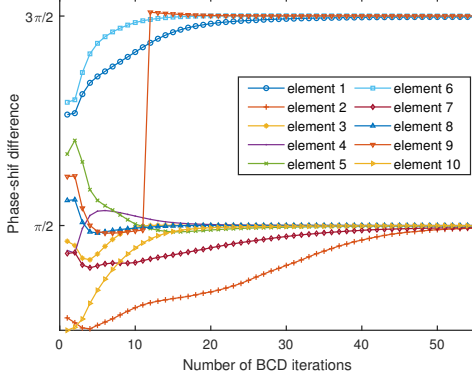


Fig. 4: Phase-shift difference in Algorithm 5 at the first iteration of PDD.

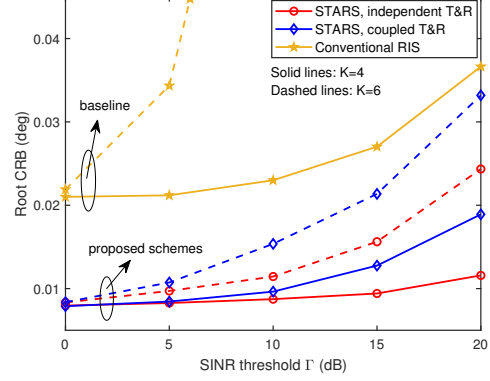


Fig. 5: Root CRB achieved by different schemes versus communication SINR threshold Γ .

fixed number of elements for sensing and communication spaces and therefore cannot achieve the same DoFs as STARS. Furthermore, there is only a slight performance gap between the coupled and independent phase-shift when the communication requirements are weak. The reason behind this can be explained as follows. In the extreme case where communication SINR threshold approaches to zero, namely $\Gamma \rightarrow 0$, all power will be split to the sensing space for enhancing the sensing estimation performance, namely $\beta_{t,n} \rightarrow 1$ and $\beta_{r,n} \rightarrow 0, \forall n \in \mathcal{N}$. In this case, the coupled phase-shift is automatically satisfied, which is identical to the independent phase-shift. However, as the Γ increases, the transmission phase-shift for the communication space becomes more restrictive, which also limits the DoFs of the reflection coefficient for the sensing space and leads to a larger performance gap.

C. Impact of Passive Elements

Fig. 6 illustrates the impact of the number of passive elements N of STARS when $N_S = 5$ and $K = 4$. It can be observed that as the number of passive elements increases, the root CRB decreases and the communication SINR threshold Γ has less influence on the CRB performance. This is because more passive elements introduce more DoFs to construct a more directional sensing beam and achieve a more flexible communication channel tuning capability. Due to the same reason, when $\Gamma = 15\text{dB}$, the root CRB achieved by the two phase-shift models finally converges to the same value as N increases. However, when $\Gamma = 0\text{dB}$, the performance of the coupled phase-shift model is always comparable to that of the independent phase-shift model.

D. Impact of Sensor Elements

In Fig. 7, we further studied the impact of the number of active sensor elements N_S when $N = 10$ and $K = 4$. We can see that all the schemes are capable of achieving higher estimation

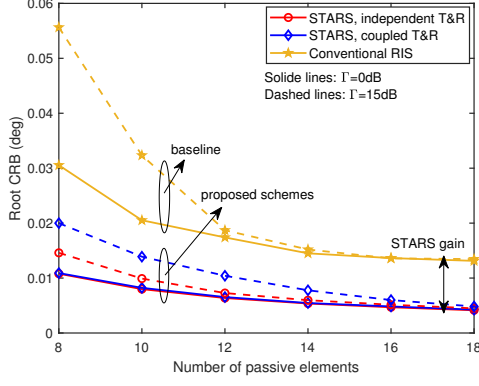


Fig. 6: Root CRB versus the number of passive elements N .

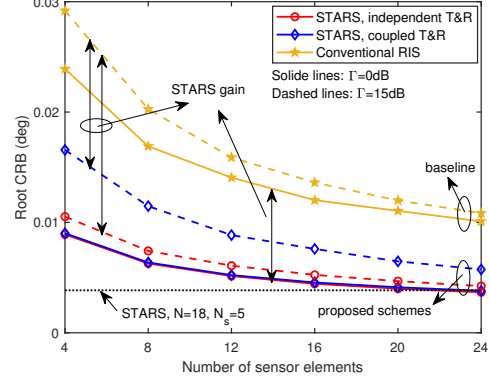


Fig. 7: Root CRB versus the number of sensor elements N_S .

accuracy when more sensor elements are installed. Similarly, the superior performance gain of STARS compared with conventional RIS is also demonstrated. When $\Gamma = 0\text{dB}$, the coupled phase-shift model achieves almost the same performance as the independent phase-shift model. When $\Gamma = 15\text{dB}$, there is a performance gap between the two phase-shift models, which is gradually reduced as the number of sensor elements increases. To obtain more insights, we also plot the achieved root CRB when $N = 18$ and $N_S = 5$, which is comparable to the root CRB achieved by the independent phase-shift model when $N = 10$ and $N_S = 24$. Moreover, the performance gap between the two phase-shift models is almost zero when $N = 18$ and $N_S = 5$, but not when $N = 10$ and $N_S = 24$. From the above, we can conclude that it is more appealing to increase the number of passive elements than to increase the number of sensor elements in terms of both system performance and manufacturing cost.

E. MLE Spectrum

To verify the effectiveness of optimizing the CRB, we implement the practical maximum likelihood estimate (MLE) of DOAs ϕ_h and ϕ_v in Appendix D. Fig. 8 demonstrates the MLE spectrum obtained via the 2D search over a predefined fine angle grid when $K = 4$. In the MLE spectrum, the point with the highest value (the brightest point) is corresponding to the estimated DOAs. As can be observed, when $\Gamma = 0\text{dB}$, STARS with both independent and coupled phase-shift can achieve a point-like brightest region around $(120^\circ, 30^\circ)$ in the spectrum, which indicates the high accuracy of estimating DOAs. When Γ increases to 20dB , the brightest region achieved by STARS with independent phase-shift is still relatively small, which is also a bit more accurate than that achieved by STARS with coupled phase-shift. However, when the conventional RIS is exploited, the brightest region becomes very large regardless of the value of Γ , leading to a

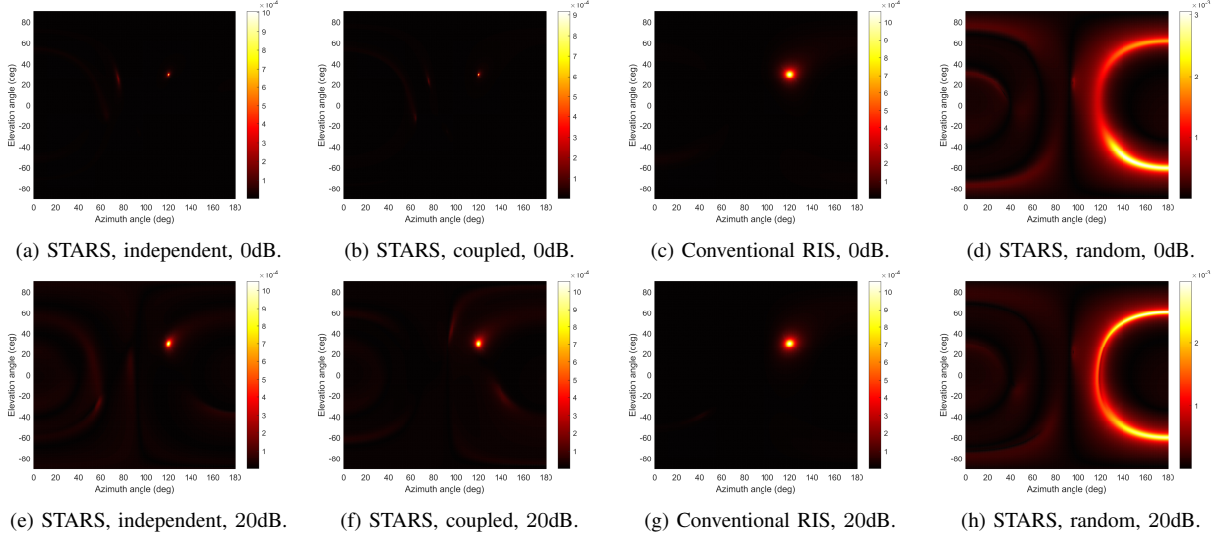


Fig. 8: Obtained MLE spectrums by different schemes when $\Gamma = 0\text{dB}$ or 20dB .

low sensing resolution. Finally, we also demonstrate the MLE spectrum obtained by the STARS with random transmission phase-shift but the communication SINR is still guaranteed, which is related to the cases without optimizing the CRB. In this case, we can see that the estimation of DOAs is almost infeasible, which verifies the effectiveness of optimizing the CRB.

VI. CONCLUSION

A STARS-enabled ISAC system was investigated, where a novel sensing-at-STARS structure and two efficient CRB optimization frameworks for both independent and coupled T&R phase-shift models were proposed. Numerical results revealed the significant performance gain of CRB and 2D DOAs estimation achieved by the STARS over the conventional RIS, and the slight performance gap between the independent and coupled T&R phase-shift models in the cases of low communication requirements and sufficient STARS elements. Moreover, compared with employing more sensor elements, installing more passive elements is more efficient in practice to enhance performance and reduce cost. This paper confirmed the effectiveness of employing STARS to simultaneously support high-quality sensing on one side and high-quality communication on the other. Consequently, in practical design, STARS is capable of breaking the physical blockage such as walls and windows, extending the legacy communication or sensing system, and carrying out the other function in a separate space. Finally, the potential of STARS to support dual functions on both sides is also foreseeable, which can be a promising direction for future research.

APPENDIX A: DERIVATION OF THE FISHER INFORMATION MATRICES

Firstly, we have

$$\frac{\partial \mathbf{u}}{\partial \phi} = [\alpha \text{vec}(\dot{\mathbf{B}}_{\phi_h} \boldsymbol{\Theta}_r \mathbf{H} \mathbf{X}), \alpha \text{vec}(\dot{\mathbf{B}}_{\phi_v} \boldsymbol{\Theta}_r \mathbf{H} \mathbf{X})], \quad \frac{\partial \mathbf{u}}{\partial \tilde{\alpha}} = \text{vec}(\mathbf{B} \boldsymbol{\Theta}_r \mathbf{H} \mathbf{X})[1, j]. \quad (\text{A.1})$$

Here, $\mathbf{B} = \mathbf{b}(\phi_h, \phi_v) \mathbf{a}^T(\phi_h, \phi_v)$ and $\dot{\mathbf{B}}_{\phi_p} = \frac{\partial \mathbf{B}}{\partial \phi_p}$, which is derived by

$$\dot{\mathbf{B}}_{\phi_h} = \frac{\partial \mathbf{b}}{\partial \phi_h} \mathbf{a}^T + \mathbf{b} \frac{\partial \mathbf{a}^T}{\partial \phi_h} = j \frac{2\pi}{\lambda_c} \sin \phi_h \cos \phi_v ((\bar{\mathbf{r}}_X \odot \mathbf{b}) \mathbf{a}^T(\phi_h, \phi_v) + \mathbf{b}(\mathbf{r}_X \odot \mathbf{a})^T). \quad (\text{A.2})$$

$$\begin{aligned} \dot{\mathbf{B}}_{\phi_v} &= \frac{\partial \mathbf{b}}{\partial \phi_v} \mathbf{a}^T + \mathbf{b} \frac{\partial \mathbf{a}^T}{\partial \phi_v} \\ &= j \frac{2\pi}{\lambda_c} \cos \phi_h \sin \phi_v ((\bar{\mathbf{r}}_X \odot \mathbf{b}) \mathbf{a}^T(\phi_h, \phi_v) + \mathbf{b}(\mathbf{r}_X \odot \mathbf{a})^T) - j \frac{2\pi}{\lambda_c} \cos \phi_v \mathbf{b}(\mathbf{r}_Z \odot \mathbf{a})^T, \end{aligned} \quad (\text{A.3})$$

where we drop ϕ_h and ϕ_v in \mathbf{b} and \mathbf{a} for notational convenience. Then, $\mathbf{J}_{\phi\phi}$ can be further partitioned as

$$\mathbf{J}_{\phi\phi} = \begin{bmatrix} J_{\phi_h \phi_h} & J_{\phi_h \phi_v} \\ J_{\phi_h \phi_v} & J_{\phi_v \phi_v} \end{bmatrix}. \quad (\text{A.4})$$

Then, according to (16), the entries of $\mathbf{J}_{\phi\phi}$ can be calculated as follows:

$$\begin{aligned} J_{\phi_l \phi_p} &= \frac{2}{\sigma_s^2} \text{Re} \left\{ \alpha^* \text{vec}(\dot{\mathbf{B}}_{\phi_l} \boldsymbol{\Theta}_r \mathbf{H} \mathbf{X})^H \alpha \text{vec}(\dot{\mathbf{B}}_{\phi_p} \boldsymbol{\Theta}_r \mathbf{H} \mathbf{X}) \right\} \\ &= \frac{2|\alpha|^2 L}{\sigma_s^2} \text{Re} \left\{ \text{tr}(\dot{\mathbf{B}}_{\phi_p} \boldsymbol{\Theta}_r \mathbf{H} \mathbf{R}_X \mathbf{H}^H \boldsymbol{\Theta}_r^H \dot{\mathbf{B}}_{\phi_l}^H) \right\}, \forall l, p \in \{h, v\}. \end{aligned} \quad (\text{A.5})$$

Next, the matrices $\mathbf{J}_{\phi\tilde{\alpha}}$ and $\mathbf{J}_{\tilde{\alpha}\tilde{\alpha}}$ are derived, which are given by

$$\begin{aligned} \mathbf{J}_{\phi\tilde{\alpha}} &= \frac{2}{\sigma_s^2} \text{Re} \left(\begin{bmatrix} \alpha^* \text{vec}(\dot{\mathbf{B}}_{\phi_h} \boldsymbol{\Theta}_r \mathbf{H} \mathbf{X})^H \\ \alpha^* \text{vec}(\dot{\mathbf{B}}_{\phi_v} \boldsymbol{\Theta}_r \mathbf{H} \mathbf{X})^H \end{bmatrix} \text{vec}(\mathbf{B} \boldsymbol{\Theta}_r \mathbf{H} \mathbf{X})[1, j] \right) \\ &= \frac{2L}{\sigma_s^2} \text{Re} \left(\begin{bmatrix} \alpha^* \text{tr}(\mathbf{B} \boldsymbol{\Theta}_r \mathbf{H} \mathbf{R}_X \mathbf{H}^H \boldsymbol{\Theta}_r^H \dot{\mathbf{B}}_{\phi_h}^H) \\ \alpha^* \text{tr}(\mathbf{B} \boldsymbol{\Theta}_r \mathbf{H} \mathbf{R}_X \mathbf{H}^H \boldsymbol{\Theta}_r^H \dot{\mathbf{B}}_{\phi_v}^H) \end{bmatrix} [1, j] \right). \end{aligned} \quad (\text{A.6})$$

$$\begin{aligned} \mathbf{J}_{\tilde{\alpha}\tilde{\alpha}} &= \frac{2}{\sigma_s^2} \text{Re} ((\text{vec}(\mathbf{B} \boldsymbol{\Theta}_r \mathbf{H} \mathbf{X})[1, j])^H \text{vec}(\mathbf{B} \boldsymbol{\Theta}_r \mathbf{H} \mathbf{X})[1, j]) \\ &= \frac{2}{\sigma_s^2} \text{Re} ([1, j]^H [1, j] \text{vec}(\mathbf{B} \boldsymbol{\Theta}_r \mathbf{H} \mathbf{X})^H \text{vec}(\mathbf{B} \boldsymbol{\Theta}_r \mathbf{H} \mathbf{X})) \\ &= \frac{2L}{\sigma_s^2} \mathbf{I}_2 \text{tr}(\mathbf{B} \boldsymbol{\Theta}_r \mathbf{H} \mathbf{R}_X \mathbf{H}^H \boldsymbol{\Theta}_r^H \mathbf{B}^H) \end{aligned} \quad (\text{A.7})$$

APPENDIX B: PROOF OF PROPOSITION 3

For any given $\tilde{\beta}_t$ and $\tilde{\beta}_r$, the optimization problem with respect to $\tilde{\mathbf{q}}_t$ and $\tilde{\mathbf{q}}_r$ is given by

$$\min_{\tilde{\mathbf{q}}_t, \tilde{\mathbf{q}}_r} \text{Re}(\tilde{\boldsymbol{\vartheta}}_t^H \tilde{\mathbf{q}}_t) + \text{Re}(\tilde{\boldsymbol{\vartheta}}_r^H \tilde{\mathbf{q}}_r) \quad (\text{B.1a})$$

$$\text{s.t. } [\tilde{\mathbf{q}}_r]_n = j[\tilde{\mathbf{q}}_t]_n \text{ or } [\tilde{\mathbf{q}}_r]_n = -j[\tilde{\mathbf{q}}_t]_n, \forall n \in \mathcal{N}, \quad (\text{B.1b})$$

$$|[\tilde{\mathbf{q}}_t]_n| = 1, |[\tilde{\mathbf{q}}_r]_n| = 1, \forall n \in \mathcal{N}, \quad (\text{B.1c})$$

where constraint (B.1b) is transformed from the coupled T&R phase-shift constraint (55c). It can be observed this problem is a separable optimization problem. In other words, each pair of $(\tilde{q}_{t,n}, \tilde{q}_{r,n})$ can be optimized individually, the related optimization problem of which is given by

$$\min_{\tilde{q}_{t,n}, \tilde{q}_{r,n}} \text{Re}(\tilde{\vartheta}_{t,n}^* \tilde{q}_{t,n}) + \text{Re}(\tilde{\vartheta}_{r,n}^* \tilde{q}_{r,n}) \quad (\text{B.2a})$$

$$\text{s.t. } \tilde{q}_{r,n} = j\tilde{q}_{t,n} \text{ or } \tilde{q}_{r,n} = -j\tilde{q}_{t,n}, \quad (\text{B.2b})$$

$$|\tilde{q}_{t,n}| = 1, |\tilde{q}_{r,n}| = 1. \quad (\text{B.2c})$$

Substituting the constraint (B.2b) into the objective function, the above problem can be further simplified as $\min_{|\tilde{q}_{t,n}|=1} \text{Re}((\tilde{\vartheta}_{t,n}^* \pm j\tilde{\vartheta}_{r,n}^*)\tilde{q}_{t,n})$, where the factor $(\tilde{\vartheta}_{t,n}^* + j\tilde{\vartheta}_{r,n}^*)$ is for the case $\tilde{q}_{r,n} = j\tilde{q}_{t,n}$ and the factor $(\tilde{\vartheta}_{t,n}^* - j\tilde{\vartheta}_{r,n}^*)$ is for the case $\tilde{q}_{r,n} = -j\tilde{q}_{t,n}$. It is clear that the optimal $\tilde{q}_{t,n}$ should such that the phase of $(\tilde{\vartheta}_{t,n}^* \pm j\tilde{\vartheta}_{r,n}^*)\tilde{q}_{t,n}$ to be π , yielding the following optimal solution:

$$\tilde{q}_{t,n} = e^{j(\pi - \angle(\tilde{\vartheta}_{t,n}^* \pm j\tilde{\vartheta}_{r,n}^*))}, \quad (\text{B.3})$$

By matching the optimal $\tilde{q}_{t,n}$ with the cases of $\tilde{q}_{r,n} = j\tilde{q}_{t,n}$ and $\tilde{q}_{r,n} = -j\tilde{q}_{t,n}$, the solutions in (59) can be obtained, which completes the proof.

APPENDIX C: PROOF OF PROPOSITION 4

For any given $\tilde{\mathbf{q}}_t$ and $\tilde{\mathbf{q}}_r$, the optimization problem with respect to $\tilde{\boldsymbol{\beta}}_t$ and $\tilde{\boldsymbol{\beta}}_r$ is given by

$$\min_{\tilde{\boldsymbol{\beta}}_t, \tilde{\boldsymbol{\beta}}_r} \text{Re}(\check{\boldsymbol{\vartheta}}_t^H \tilde{\boldsymbol{\beta}}_t) + \text{Re}(\check{\boldsymbol{\vartheta}}_r^H \tilde{\boldsymbol{\beta}}_r) \quad (\text{C.1a})$$

$$\text{s.t. } \tilde{\beta}_{t,n}^2 + \tilde{\beta}_{r,n}^2 = 1, 0 \leq \tilde{\beta}_{t,n}, \tilde{\beta}_{r,n} \leq 1, \forall n \in \mathcal{N}, \quad (\text{C.1b})$$

which is also a separable problem. The separated problem related to $\tilde{\beta}_{t,n}$ and $\tilde{\beta}_{r,n}$ is given by

$$\min_{\tilde{\beta}_{t,n}, \tilde{\beta}_{r,n}} g_n = \text{Re}(\check{\vartheta}_{t,n}^* \tilde{\beta}_{t,n}) + \text{Re}(\check{\vartheta}_{r,n}^* \tilde{\beta}_{r,n}) \quad (\text{C.2a})$$

$$\text{s.t. } \tilde{\beta}_{t,n}^2 + \tilde{\beta}_{r,n}^2 = 1, 0 \leq \tilde{\beta}_{t,n}, \tilde{\beta}_{r,n} \leq 1, \quad (\text{C.2b})$$

where $\check{\vartheta}_{i,n}, \forall i \in \{t, r\}$ denotes the n -th entry of $\check{\boldsymbol{\vartheta}}_i$. Since $\tilde{\beta}_{i,n}, \forall i \in \{t, r\}$ is real, the objective function can be further simplified as $a_n \tilde{\beta}_{t,n} + b_n \tilde{\beta}_{r,n}$, where $a_n = |\check{\vartheta}_{t,n}^*| \cos(\angle \check{\vartheta}_{t,n}^*)$ and $b_n = |\check{\vartheta}_{r,n}^*| \cos(\angle \check{\vartheta}_{r,n}^*)$. In this case, problem (C.2) is essentially to find the minimum value of the real function $a_n \tilde{\beta}_{t,n} + b_n \tilde{\beta}_{r,n}$ on the unit circle $\tilde{\beta}_{t,n}^2 + \tilde{\beta}_{r,n}^2 = 1$ in the first quadrant. To solve it, we transform it to the polar coordinate system by letting $\tilde{\beta}_{t,n} = \sin \omega_n$ and $\tilde{\beta}_{r,n} = \cos \omega_n$ with $\omega_n \in [0, \frac{1}{2}\pi]$. Then, the objective function can be rewritten as

$$\begin{aligned}
g_n &= a_n \sin \omega_n + b_n \cos \omega_n \stackrel{(a)}{=} \sqrt{a_n^2 + b_n^2} (\cos \psi_n \sin \omega_n + \sin \psi_n \cos \omega_n) \\
&= \sqrt{a_n^2 + b_n^2} \sin(\omega_n + \psi_n),
\end{aligned} \tag{C.3}$$

where the equality (a) is achieved by defining $\cos \psi_n = \frac{a_n}{\sqrt{a_n^2 + b_n^2}}$ and $\sin \psi_n = \frac{b_n}{\sqrt{a_n^2 + b_n^2}}$. As a consequence, the problem is to find the minimum value of $\sin(\omega_n + \psi_n)$ with respect to ω_n in the interval $[0, \frac{1}{2}\pi]$. Thus, the optimal ω_n in (61) can be readily obtained. Based on this, the optimal $\tilde{\beta}_{t,n}$ and $\tilde{\beta}_{r,n}$ can also be obtained, which completes the proof.

APPENDIX D: MAXIMUM LIKELIHOOD ESTIMATE OF DOAs

According to (15), the vectorized signal over the sensing dwell time L at the sensor can be rewritten as

$$\mathbf{y}_s = \alpha \boldsymbol{\delta}(\phi_h, \phi_v) + \mathbf{n}_s, \tag{D.1}$$

where $\boldsymbol{\delta}(\phi_h, \phi_v) = \text{vec}(\mathbf{b}(\phi_h, \phi_v) \mathbf{a}^T(\phi_h, \phi_v) \boldsymbol{\Theta}_r \mathbf{H} \mathbf{X})$. It can be observed that \mathbf{y}_s is a Gaussian vector with mean $\alpha \boldsymbol{\delta}(\phi_h, \phi_v)$ and variance $\sigma_s \mathbf{I}_{N_s L}$. Given parameters $\boldsymbol{\xi}$, the likelihood function of \mathbf{y}_s is

$$f_{\mathbf{y}_s}(\mathbf{y}_s; \boldsymbol{\xi}) = \frac{1}{\sqrt{(\pi \sigma_s)^{N_s L}}} \exp \left(-\frac{1}{\sigma^2} \|\mathbf{y}_s - \alpha \boldsymbol{\delta}(\phi_h, \phi_v)\|^2 \right). \tag{D.2}$$

Thus, the MLE of $\boldsymbol{\xi}$ is given by

$$\hat{\boldsymbol{\xi}} = \arg \max_{\boldsymbol{\xi}} f_{\mathbf{y}_s}(\mathbf{y}_s; \boldsymbol{\xi}) = \arg \min_{\boldsymbol{\xi}} \|\mathbf{y}_s - \alpha \boldsymbol{\delta}(\phi_h, \phi_v)\|^2. \tag{D.3}$$

According to (D.3), for any given ϕ_h and ϕ_v , α can be estimated as

$$\hat{\alpha} = \arg \min_{\alpha} \|\mathbf{y}_s - \alpha \boldsymbol{\delta}(\phi_h, \phi_v)\|^2 = \frac{\boldsymbol{\delta}^H(\phi_h, \phi_v) \mathbf{y}_s}{\|\boldsymbol{\delta}(\phi_h, \phi_v)\|^2}. \tag{D.4}$$

With $\hat{\alpha}$ at hand, we have

$$\|\mathbf{y}_s - \hat{\alpha} \boldsymbol{\delta}(\phi_h, \phi_v)\|^2 = \|\mathbf{y}_s\|^2 - \frac{|\boldsymbol{\delta}^H(\phi_h, \phi_v) \mathbf{y}_s|^2}{\|\boldsymbol{\delta}(\phi_h, \phi_v)\|^2}. \tag{D.5}$$

Thus, the MLE of ϕ_h and ϕ_v is given by

$$(\hat{\phi}_h, \hat{\phi}_v) = \arg \max_{\phi_h, \phi_v} \frac{|\boldsymbol{\delta}^H(\phi_h, \phi_v) \mathbf{y}_s|^2}{\|\boldsymbol{\delta}(\phi_h, \phi_v)\|^2}, \tag{D.6}$$

which can be obtained by exhaustively searching ϕ_h and ϕ_v .

REFERENCES

- [1] F. Liu, Y. Cui, C. Masouros, J. Xu, T. X. Han, Y. C. Eldar, and S. Buzzi, "Integrated sensing and communications: Towards dual-functional wireless networks for 6G and beyond," *IEEE J. Sel. Areas Commun.*, vol. 40, no. 6, pp. 1728–1767, Jun. 2012.
- [2] J. A. Zhang, M. L. Rahman, K. Wu, X. Huang, Y. J. Guo, S. Chen, and J. Yuan, "Enabling joint communication and radar sensing in mobile networks—a survey," *IEEE Commun. Surv. Tut.*, vol. 24, no. 1, pp. 306–345, 1st Quart. 2021.
- [3] M. Xu, W. C. Ng, W. Y. B. Lim, J. Kang, Z. Xiong, D. Niyato, Q. Yang, X. S. Shen, and C. Miao, "A full dive into realizing the edge-enabled Metaverse: Visions, enabling technologies, and challenges," *arXiv preprint arXiv:2203.05471*, 2022.
- [4] Y. Liu, X. Liu, X. Mu, T. Hou, J. Xu, M. Di Renzo, and N. Al-Dhahir, "Reconfigurable intelligent surfaces: Principles and opportunities," *IEEE Commun. Surv. Tut.*, vol. 23, no. 3, pp. 1546–1577, 3rd Quart. 2021.

- [5] Y. Liu, X. Mu, J. Xu, R. Schober, Y. Hao, H. V. Poor, and L. Hanzo, "STAR: Simultaneous transmission and reflection for 360° coverage by intelligent surfaces," *IEEE Wireless Commun.*, vol. 28, no. 6, pp. 102–109, Dec. 2021.
- [6] X. Mu, Y. Liu, L. Guo, J. Lin, and R. Schober, "Simultaneously transmitting and reflecting (STAR) RIS aided wireless communications," *IEEE Trans. Wireless Commun.*, vol. 21, no. 5, pp. 3083–3098, May 2022.
- [7] F. Liu, C. Masouros, A. Li, H. Sun, and L. Hanzo, "MU-MIMO communications with MIMO radar: From co-existence to joint transmission," *IEEE Trans. Wireless Commun.*, vol. 17, no. 4, pp. 2755–2770, Apr. 2018.
- [8] X. Liu, T. Huang, N. Shlezinger, Y. Liu, J. Zhou, and Y. C. Eldar, "Joint transmit beamforming for multiuser MIMO communications and MIMO radar," *IEEE Trans. Signal Process.*, vol. 68, pp. 3929–3944, Jun. 2020.
- [9] J. Pritzker, J. Ward, and Y. C. Eldar, "Transmit precoder design approaches for dual-function radar-communication systems," *arXiv preprint arXiv:2203.09571*, 2022.
- [10] H. Zhang, H. Zhang, B. Di, M. Di Renzo, Z. Han, H. V. Poor, and L. Song, "Holographic integrated sensing and communication," *IEEE J. Sel. Areas Commun.*, Jul. 2022.
- [11] L. Chen, Z. Wang, Y. Du, Y. Chen, and F. R. Yu, "Generalized transceiver beamforming for DFRC with MIMO radar and MU-MIMO communication," *IEEE J. Sel. Areas Commun.*, vol. 40, no. 6, pp. 1795–1808, Jun. 2022.
- [12] C. Ouyang, Y. Liu, and H. Yang, "Performance of downlink and uplink integrated sensing and communications (ISAC) systems," *IEEE Wireless Commun. Lett.*, early access, Jun. 2021, doi: 10.1109/LWC.2022.3184409.
- [13] F. Liu, Y.-F. Liu, A. Li, C. Masouros, and Y. C. Eldar, "Cramér-Rao bound optimization for joint radar-communication beamforming," *IEEE Trans. Signal Process.*, vol. 70, pp. 240–253, Dec. 2021.
- [14] H. Hua, X. Song, Y. Fang, T. X. Han, and J. Xu, "MIMO integrated sensing and communication with extended target: CRB-Rate tradeoff," *arXiv preprint arXiv:2205.14050*, 2022.
- [15] C. Huang, A. Zappone, G. C. Alexandropoulos, M. Debbah, and C. Yuen, "Reconfigurable intelligent surfaces for energy efficiency in wireless communication," *IEEE Trans. Wireless Commun.*, vol. 18, no. 8, pp. 4157–4170, Aug. 2019.
- [16] Q. Wu and R. Zhang, "Intelligent reflecting surface enhanced wireless network via joint active and passive beamforming," *IEEE Trans. Wireless Commun.*, vol. 18, no. 11, pp. 5394–5409, Nov. 2019.
- [17] X. Yu, D. Xu, D. W. K. Ng, and R. Schober, "IRS-assisted green communication systems: Provable convergence and robust optimization," *IEEE Trans. Commun.*, vol. 69, no. 9, pp. 6313–6329, Sep. 2021.
- [18] H. Zhang, H. Zhang, B. Di, K. Bian, Z. Han, and L. Song, "MetaRadar: Multi-target detection for reconfigurable intelligent surface aided radar systems," *IEEE Trans. Wireless Commun.*, early access, Mar. 2022, doi: 10.1109/TWC.2022.3153792.
- [19] X. Shao, C. You, W. Ma, X. Chen, and R. Zhang, "Target sensing with intelligent reflecting surface: Architecture and performance," *IEEE J. Sel. Areas Commun.*, vol. 40, no. 7, pp. 2070–2084, Mar. 2022.
- [20] X. Song, J. Xu, F. Liu, T. X. Han, and Y. C. Eldar, "Intelligent reflecting surface enabled sensing: Cramér-Rao lower bound optimization," *arXiv preprint arXiv:2204.11071*, 2022.
- [21] R. Sankar, S. P. Chepuri, and Y. C. Eldar, "Beamforming in integrated sensing and communication systems with reconfigurable intelligent surfaces," *arXiv preprint arXiv:2206.07679*, 2022.
- [22] R. Liu, M. Li, Y. Liu, Q. Wu, and Q. Liu, "Joint transmit waveform and passive beamforming design for RIS-aided DFRC systems," *IEEE J. Sel. Topics Signal Process.*, early access, May 2022, doi: 10.1109/JSTSP.2022.3172788.
- [23] X. Wang, Z. Fei, J. Huang, and H. Yu, "Joint waveform and discrete phase shift design for RIS-assisted integrated sensing and communication system under Cramér-Rao bound constraint," *IEEE Trans. Veh. Technol.*, vol. 71, no. 1, pp. 1004–1009, Jan. 2022.
- [24] J. Xu, Y. Liu, X. Mu, R. Schober, and H. V. Poor, "STAR-RISs: A correlated T&R phase-shift model and practical phase-shift configuration strategies," *IEEE J. Sel. Topics Signal Process.*, early access, May. 2022, doi:10.1109/JSTSP.2022.3175030.
- [25] A. Manikas, *Differential geometry in array processing*. London, UK: Imperial College Press, 2004.
- [26] S. M. Kay, *Fundamentals of statistical signal processing: estimation theory*. Englewood Cliffs, NJ: Prentice-Hall, 1993.
- [27] I. Bekkerman and J. Tabrikian, "Target detection and localization using MIMO radars and sonars," *IEEE Trans. Signal Process.*, vol. 54, no. 10, pp. 3873–3883, Oct. 2006.
- [28] S. Boyd, S. P. Boyd, and L. Vandenberghe, *Convex optimization*. Cambridge, U.K.: Cambridge university press, 2004.
- [29] F. Zhang, *The Schur Complement and Its Applications*. Berlin, Germany: Springer-Verlag, 2005.
- [30] Q. Shi and M. Hong, "Penalty dual decomposition method for nonsmooth nonconvex optimization—Part I: Algorithms and convergence analysis," *IEEE Trans. Signal Process.*, vol. 68, pp. 4108–4122, Jun. 2020.
- [31] Z.-Q. Luo, W.-K. Ma, A. M.-C. So, Y. Ye, and S. Zhang, "Semidefinite relaxation of quadratic optimization problems," *IEEE Signal Process. Mag.*, vol. 27, no. 3, pp. 20–34, May 2010.
- [32] M. Razaviyayn, M. Hong, and Z.-Q. Luo, "A unified convergence analysis of block successive minimization methods for nonsmooth optimization," *SIAM J. Optim.*, vol. 23, no. 2, pp. 1126–1153, 2013.
- [33] K.-C. Toh, "An inexact primal–dual path following algorithm for convex quadratic SDP," *Math. Program.*, vol. 112, no. 1, pp. 221–254, 2008.